Journal of the Mechanics and Physics of Solids 97 (2016) 275–298

Contents lists available at ScienceDirect

Journal of the Mechanics and Physics of Solids

journal homepage: www.elsevier.com/locate/jmps

Localization of deformation and loss of macroscopic ellipticity in microstructured solids

M.P. Santisi d'Avila [a], N. Triantafyllidis [b,c,d,*], G. Wen [b]

[a] Laboratoire J.A.Dieudonné, C.N.R.S. UMR 7351 Université de Nice Sophia-Antipolis, Nice 06108, France
[b] Laboratoire de Mécanique des Solides, C.N.R.S. UMR 7649 École Polytechnique, Palaiseau 91128, France
[c] Département de Mécanique, École Polytechnique, Palaiseau 91128, France
[d] Aerospace Engineering Department & Mechanical Engineering Department (emeritus), The University of Michigan, Ann Arbor, MI 48109-2140, USA

ARTICLE INFO

Article history:
Received 22 April 2016
Received in revised form
21 June 2016
Accepted 7 July 2016
Available online 11 July 2016

Keywords:
Nonlinear Elasticity
Composites
Bifurcation
Instabilities
Homogenization
Cellular Solids

ABSTRACT

Localization of deformation, a precursor to failure in solids, is a crucial and hence widely studied problem in solid mechanics. The continuum modeling approach of this phenomenon studies conditions on the constitutive laws leading to the loss of ellipticity in the governing equations, a property that allows for discontinuous equilibrium solutions. Micro-mechanics models and nonlinear homogenization theories help us understand the origins of this behavior and it is thought that a loss of macroscopic (homogenized) ellipticity results in localized deformation patterns. Although this is the case in many engineering applications, it raises an interesting question: is there always a localized deformation pattern appearing in solids losing macroscopic ellipticity when loaded past their critical state?

In the interest of relative simplicity and analytical tractability, the present work answers this question in the restrictive framework of a layered, nonlinear (hyperelastic) solid in plane strain and more specifically under axial compression along the lamination direction. The key to the answer is found in the homogenized post-bifurcated solution of the problem, which for certain materials is supercritical (increasing force and displacement), leading to post-bifurcated equilibrium paths in these composites that show no localization of deformation for macroscopic strain well above the one corresponding to loss of ellipticity.

1. Introduction

Localization of deformation in finitely strained ductile solids is the instability mechanism leading to failure by rupture. The general principles were introduced for the study of this fascinating and important for applications phenomenon in the context of continuum mechanics by Hadamard (1903) and subsequently advanced in his spirit by Hill (1962), Mandel (1966) and Rice (1976). The underlying mathematical concept in the continuum model is the loss of ellipticity in the governing equations, which allows for discontinuous strain solutions. With the advent of homogenization theories since the 1960s,a vast amount of work has been dedicated to the bridging of scales and understanding how micromechanical features in

* Corresponding author at: Laboratoire de Mécanique des Solides, C.N.R.S. UMR 7649 École Polytechnique, Palaiseau 91128, France.
E-mail address: nick@lms.polytechnique.fr (N. Triantafyllidis).

http://dx.doi.org/10.1016/j.jmps.2016.07.009
0022-5096/

solids lead to their macroscopic (homogenized) loss of ellipticity at adequate levels of strain or stress. A plethora of applications for a wide range of solids has appeared in the literature, covering rubber elasticity, various types of composites (porous, fiber-reinforced, particle-reinforced, cellular solids, etc.), metal plasticity, granular media, rocks, just to name a few. Since the review of such a large and diverse body of work is unfortunately not possible, only key references relevant to the points made in the present article will be cited.

To avoid difficulties related to microstructure geometry and the identification of associated scale and representative volume, our attention is restricted to solids with a well defined scale, i.e. to architectured materials with periodic microsctructures. The role played by buckling at the microscopic scale, as the onset of instability mechanism leading to macroscopic localization of deformation in these materials has been established and subsequently analyzed by a long series of investigations. For the case of fiber reinforced composites, the connection between local buckling and global localization started with the work of Rosen (1965), who recognized microbuckling as the onset of instability mechanism. Subsequent investigations of Budiansky (1983), Budiansky and Fleck (1993), Kyriakides et al. (1995), Vogler et al. (2001) and many others showed, with progressively more sophisticated experiments and detailed modeling, how the buckling instability evolves into a localized deformation pattern (kinkband formation) and studied in detail the characteristics of these bands. The same basic mechanism, i.e. buckling initiated at the microstructural level, has been recognized in materials science as the cause for localization of deformation in cellular solids (crushing zones) and the interested reader is referred to the comprehensive monograph by Gibson and Ashby (1988). Detailed experimental and theoretical investigations followed in mechanics with a particular interest in studying the initiation and evolution towards localization of the deformation pattern in cellular solids by Papka and Kyriakides (1994, 1998, 1999a, 1999b) for 2D microstructures and Jang et al. (2010), Wilbert et al. (2011) for 3D microstructures and in establishing conditions where local or global buckling is the critical mechanism at the onset of failure by Triantafyllidis and Schraad (1998), Gong et al. (2005), and Lopez-Jimenez and Triantafyllidis (2013).

Progressing in parallel, the nonlinear homogenization theories that appeared in mechanics first addressed questions on macroscopic response in plasticity, viscoelasticity and nonlinear elasticity with various microstructures (e.g. see Suquet, 1983; Talbot and Willis, 1985; Ponte Castañeda, 1991) and subsequently explored localization of deformation issues (e.g. see Kailasam and Ponte Castañeda, 1998; Lopez-Pamies and Ponte Castañeda, 2004). For periodic solids the question asked was the possibility of detecting instabilities at the microscopic level from their homogenized properties, thus formally connecting buckling at the microscopic level to localization of deformation. For these composites it has been shown, initially for layered solids by Triantafyllidis and Maker (1985) and subsequently for the general 3D periodic case by Geymonat et al. (1993), that microstructural bifurcation phenomena (micro-buckling) is the mechanism responsible for macroscopic loss of ellipticity and that a long wavelength critical mode (based on Bloch wave analysis of the perfect infinite composite) coincides with the loss of ellipticity in its homogenized incremental moduli. Further work for porous elastomers by Michel et al. (2007) and for particle reinforced elastomers by Michel et al. (2010) has been done to connect local buckling to the macroscopic loss of ellipticity and compare periodic to random isotropic media with the same volume fractions.

Since loss of ellipticity is the property allowing for discontinuous equilibrium solutions, it is thought (and supported by micromechanical calculations in most of the known—to the best of our knowledge—engineering applications), that a loss of macroscopic (homogenized) ellipticity results in a localized deformation pattern in the post-bifurcated regime. However, an interesting question arises: is there always a localized deformation appearing in the post-bifurcation of solids losing macroscopic ellipticity and what are the necessary conditions in the homogenized response leading to localization?

In the interest of relative simplicity and analytical tractability, the present work answers these questions in the restrictive framework of an infinite, layered, nonlinear (hyperelastic) solid under plane strain loading conditions and more specifically under axial compression along the lamination direction. For this problem, based on a periodic unit cell construction, one can find macroscopic loads where the homogenized moduli of the principal solution lose ellipticity (and since the solid has an energy density, the corresponding homogenized energy loses rank-one convexity). Moreover one can also ensure that the critical (i.e. corresponding to the lowest applied load) bifurcation eigenmode of the infinite solid is global (infinite wavelength eigenmode), a property that for this problem allows us to find an homogenized solution for the post-bifurcated equilibrium path. The answer to the localization question posed lies in the homogenized, initial post-bifurcation response of the perfect layered solid, as seen in Fig. 1; it will be shown that for a composite with a monotonically increasing force (and

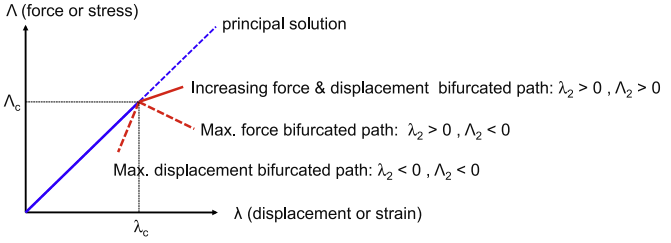

Fig. 1. Different cases for the homogenized, initial post-bifurcation behavior of a perfect, nonlinear (hyperelastic) layered composite under plane strain loading conditions which is subjected to axial compression along its lamination direction. Stable paths are marked by solid lines and unstable ones by broken lines. For a composite with a monotonically increasing force (and displacement) post-bifurcation response ($\lambda_2 > 0$, $\Lambda_2 > 0$), no localized deformation solution develops in spite of a loss of ellipticity found at the macroscopic critical strain λ_c.

displacement) post-bifurcation response ($\Lambda_2 > 0,\ \lambda_2 > 0$), no localized deformation solution develops in spite of a loss of ellipticity found at the macroscopic critical strain λ_c. The stability or instability of paths indicated in Fig. 1 pertains to whether the corresponding homogenized energy density has a local minimum or maximum with respect to the load parameter.

The presentation is organized as follows: The model of the perfect, laminated, periodic composite is presented in Section 2; more specifically the bifurcation load and corresponding eigenmode and their nature (local or global) are discussed in Section 2.1. The exact solution for the post-bifurcation equilibrium path corresponding to a global eigenmode is given in Section 2.2 while the asymptotic analysis of the homogenized post-bifurcation equilibrium path and its connection to the homogenized moduli of the composite is given in Section 2.3.

The results are presented in Section 3, starting with the choice of constitutive laws in Section 3.1 and continuing with the general homogenized solution for the post-bifurcated equilibrium path for an infinite, perfect, incompressible hyperelastic layered solid in Section 3.2. This model allows us to investigate all possible scenarios: cases under which this bifurcation involves a maximum displacement, a maximum force or a bifurcation occurring under increasing force and displacement (see Fig. 1). The case of neo-Hookean composites is presented in Section 3.3, where it is shown that they always have a stable, homogenized post-bifurcation response under increasing force and displacement. Composites with decreasing homogenized post-bifurcation force or displacement are given in Section 3.4. The important question is how an adequately large, but finite size volume of such a composite will behave is addressed in Section 3.5. It is shown, by means of introducing a small geometric imperfection at the middle of a large sample that under these *"soft"* boundary conditions, the monotonically increasing force (and displacement) composites will evolve towards a uniform shearing solution away from the macroscopic critical load and show no localization of deformation pattern past the critical load, in spite of a macroscopic loss of ellipticity; as expected the composites with the snap-through (i.e. maximum displacement) macroscopic response will evolve into a solution with a single strong localized deformation zone.

Concluding remarks are presented in Section 4. Finally some complementary material of interest is presented in Appendix: Details of the general bifurcation analysis of the infinite, perfect, rate-independent, layered composite in Appendix A, the post-bifurcation equilibrium of the compressible neo-Hookean composite in Appendix B and the influence of constitutive model choice on the critical load (i.e. comparison of the hyperelastic model with its deformation theory counterpart using the same uniaxial response) in Appendix C.

2. Modeling

This section pertains to the modeling of the onset of bifurcation and post-bifurcation response of the axially compressed hyperelastic layered solid. Finding the critical load (i.e. lowest macroscopic compressive strain or stress) at the onset of bifurcation and the corresponding eigenmode is presented in Section 2.1. The exact solution of the post-bifurcation problem for the case of a global critical eigenmode is given in Section 2.2, followed by the corresponding asymptotic solution of this problem near the critical load in Section 2.3.

2.1. Bifurcation of a layered solid in plane strain—local vs. global critical mode

The presentation starts with the solution for the plane strain bifurcation problem for an infinite, perfectly periodic, layered, hyperelastic solid. The composite is subjected to uniaxial compression along the fiber direction characterized by a monotonically increasing *"load parameter"* $\lambda \geq 0$, which designates the absolute value of the applied macroscopic strain under displacement control (or its corresponding work-conjugate stress $\Lambda \geq 0$, when force is controlled). The goal is to find the lowest critical load λ_c (or Λ_c) and corresponding eigenmode as the load parameter increases away from $\lambda=0$ (or $\Lambda=0$), which is the stress-free, reference configuration of the solid. Without loss of generality, it is assumed in this section that the composite is loaded under displacement control.

The infinite, weightless, perfectly periodic solid is composed of a self-repeating sequence of two layers, as depicted in Fig. 2a. The two layers f (fiber) and m (matrix) have initial thickness H_f and H_m in the stress-free reference configuration. The solid is deformed under finite, plane strain conditions with perfect bonding between layers which guarantees traction and displacement continuity across each interface for all possible deformations. A full Lagrangian formulation of the problem is adopted with respect to a fixed Cartesian coordinate system X_1–X_2, where X_1 is the lamination direction.

The procedure for determining the onset of the first bifurcation hinges on finding a non-trivial solution to the difference between principal and bifurcated equilibrium solutions at the onset of a bifurcation:[1]

$$\Delta\Pi_{ij,i} = 0; \quad X_1 \in \mathbb{R}, \quad X_2 \in [0, H], \tag{2.1}$$

and interface conditions:

[1] Here and subsequently, Latin indexes range from 1 to 2, unless indicated differently. Einstein's summation convention is implied over repeated indexes. Repeated indexes in parentheses are not summed, unless indicated explicitly.

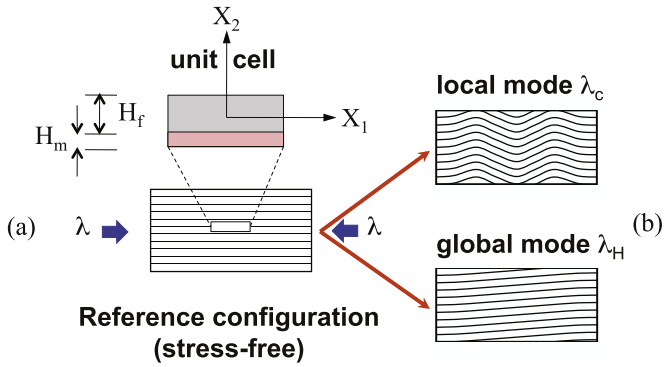

Fig. 2. Reference configuration with a unit cell in (a) and bifurcation eigenmode type (local or global) in (b), for axially compressed layered solid deformed under plane strain conditions.

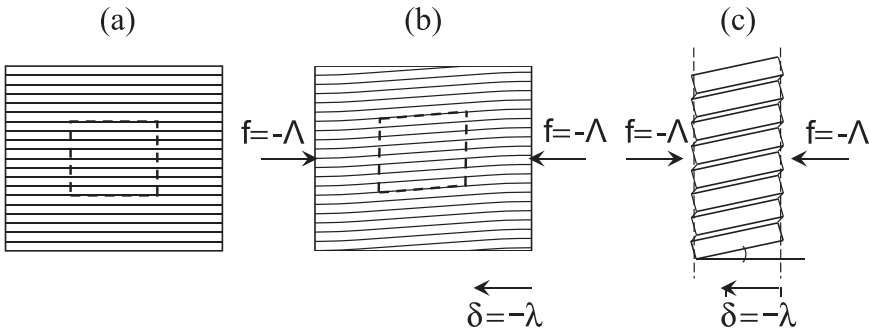

Fig. 3. Post-buckling mechanism for the case of a global critical mode in axially compressed layered media subjected to a macroscopic compressive stress $f = -\Lambda$ with a corresponding macroscopic strain $\delta = -\lambda$.

$$[\![\Delta \Pi_{2i}]\!] = 0, \quad [\![\Delta u_i]\!] = 0; \quad X_1 \in \mathbb{R}, \; X_2 \in \{0, H_m, H\}, \tag{2.2}$$

where $\Delta\boldsymbol{\Pi}$ is the difference in the first Piola–Kirchhoff stress tensors of the principal and bifurcated equilibrium solutions, $\Delta\mathbf{u}$ is the corresponding displacement field difference and $H = H_m + H_f$ is the initial thickness of the unit cell. Moreover, $[\![g]\!]$ denotes a difference in the values of any field quantity g when evaluated on both sides of an interface.

The constitutive response of the hyperelastic composite takes the form:

$$\Pi_{ji} = \frac{\partial W}{F_{ij}}, \tag{2.3}$$

where $W(\mathbf{F})$ is the strain energy density of the fiber or matrix layer and $\mathbf{F}$ is the corresponding deformation gradient. Consequently, $\Delta\boldsymbol{\Pi}$ from (2.1) can be expressed in terms of $\Delta\mathbf{u}$ by:

$$\Delta \Pi_{ji} = L_{ijkl} \Delta F_{kl}; \quad L_{ijkl} = \frac{\partial^2 W}{\partial F_{ij} \partial F_{kl}}, \quad \Delta F_{kl} = \Delta u_{k,l}. \tag{2.4}$$

The fourth rank tensor $\mathbf{L}$ is termed *"the incremental moduli tensor"* and is a function of the position $\mathbf{X}$ and the load parameter λ. The above formulation pertains to the case of a compressible solid. The slightly simpler formulation for the incompressible case has already been presented by Triantafyllidis and Maker (1985). The compressible version for the onset of bifurcation in the axially compressed, hyperelastic layered solid under plane strain is given in Geymonat et al. (1993), where the interested reader can find the complete derivations. However, for reasons of completeness of the presentation, the main results are outlined in this section and detailed derivations are given in Appendix A.

The critical load λ_c, corresponding to the onset of the first (as load parameter increases away from zero) bifurcation is found to be:

$$\lambda_c \equiv \inf_{\omega_1 H > 0} \hat{\lambda}(\omega_1 H), \tag{2.5}$$

where $\hat{\lambda}(\omega_1 H)$ is a function of the dimensionless wavenumber $\omega_1 H$ of the eigenmode along the X_1 direction, as defined in (A.14), and depends on the ratio of the two layer thicknesses and their incremental moduli $\mathbf{L}^m(\lambda)$ and $\mathbf{L}^f(\lambda)$. When the wavelength L_1 of the critical mode is commensurate with the layer thickness H, i.e. $(L_1/H)_c = 2\pi/(\omega_1 H)_c < \infty$, the critical mode

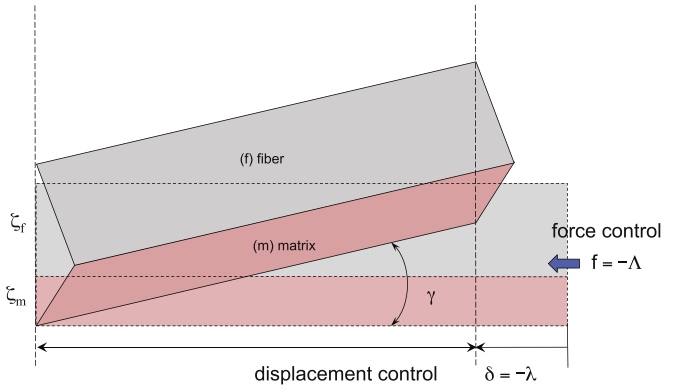

Fig. 4. Unit cell for the post-buckling equilibrium solution of an axially compressed composite with a global critical mode.

is termed *"local"*, and when this is not the case, i.e. $(L_l/H)_c = 2\pi/(\omega_1 H)_c \to \infty \Longleftrightarrow (\omega_1 H)_c \to 0$, the critical mode is termed *"global"* (see Fig. 2b). The case $(\omega_1 H)_c = 0$ corresponds to an X_1-independent solution, which is excluded by the local rank-one convexity condition for each layer, as shown in Appendix A, thus explaining the use of infimum in (2.5).

For the present work it is important to ensure that the bifurcation occurring at λ_c is global, i.e. $(\omega_1 H)_c \to 0$. In this case it can be shown that the critical load $\lambda_c = \lambda_H$, where λ_H is the lowest load corresponding to the first loss of rank-one convexity of the homogenized moduli $\mathbf{L}^H(\lambda)$ of the composite defined by:

$$\lambda_H \equiv \min_{\|\mathbf{n}\|=1} \left\{ \min \lambda > 0, \ \left| \det\left[L^H_{ijkl}(\lambda) n_j n_l \right] = 0 \right\}, \tag{2.6}$$

where the expressions for the components of the homogenized moduli $\mathbf{L}^H(\lambda)$ tensor are given in (A.21).

For all the layered composites considered here it will be shown that (2.6) is satisfied along the critical direction $(n_1, n_2)_c = (1, 0)$ and hence (due also to the orthotropy of the moduli on the principal path):

$$L^H_{2121}(\lambda_c) = 0, \tag{2.7}$$

which implies a vanishing shear stiffness of the composite at that load, perpendicular to the lamination direction.

2.2. Post-bifurcation equilibrium for global critical mode—exact solution

By ignoring the influence of boundary conditions, the onset and evolution of the long wavelength bifurcated solution emerging from $\lambda_c = \lambda_H$ is depicted in Fig. 3, according to which the initially parallel and straight layers in the principal solution in Fig. 3a evolve in a long-wavelength wavy pattern shown in Fig. 3b. The post-bifurcation equilibrium solution is idealized in Fig. 3c, according to which all layers rotate by the same angle, while each layer experiences a uniform state of strain (and stress). All fiber layers share the same strain $\mathbf{F}^f$ and all the matrix layers share $\mathbf{F}^m$, but $\mathbf{F}^f \neq \mathbf{F}^m$.

More specifically, the idealized post-buckling equilibrium is a periodic solution with a unit cell depicted in Fig. 4. This post-bifurcated equilibrium path is found as follows:

From the kinematics of deformation one has the following relations[2]:

$$\begin{aligned}
&\langle F_{11} \rangle = F^f_{11} = F^m_{11} = 1 - \lambda, \\
&\langle F_{21} \rangle = F^f_{21} = F^m_{21} = \gamma, \\
&\langle F_{12} \rangle = \zeta_f \, F^f_{12} + \zeta_m \, F^m_{12} = 0, \\
&\langle F_{22} \rangle = \zeta_f \, F^f_{22} + \zeta_m \, F^m_{22},
\end{aligned} \tag{2.8}$$

where $\zeta_f \equiv H_f/H$ and $\zeta_m \equiv H_m/H$ are respectively the volume fractions of the fiber and matrix.

From equilibrium we obtain the following relations for $\langle \Pi_{ji} \rangle$, the average first Piola–Kirchhoff stresses which are work-conjugate to $\langle F_{ij} \rangle$:

[2] Henceforth $\langle g \rangle \equiv \zeta_f g^f + \zeta_m g^m$ denotes the weighted average of a function g with different values of the fiber and matrix part of the composite.

$$\langle \Pi_{11} \rangle = \zeta_f \, \Pi_{11}^f + \zeta_m \, \Pi_{11}^m = \, -\Lambda,$$

$$\langle \Pi_{12} \rangle = \zeta_f \, \Pi_{12}^f + \zeta_m \, \Pi_{12}^m = 0,$$

$$\langle \Pi_{21} \rangle = \Pi_{21}^f = \Pi_{21}^m,$$

$$\langle \Pi_{22} \rangle = \Pi_{22}^f = \Pi_{22}^m = 0. \tag{2.9}$$

The above relations reflect the fact that the bifurcated configuration is subjected to an average compressive axial stress ($\langle \Pi_{11} \rangle = \, -\Lambda < 0$) along the X_1-direction, zero average shear stress ($\langle \Pi_{12} \rangle = 0$) and zero lateral normal stress ($\langle \Pi_{22} \rangle = 0$). To complete the above system of Eqs. (2.8) and (2.9), one has to add the constitutive response of the fiber and matrix, given by (2.3). A closed-form analytical solution is possible only for simple constitutive laws, as detailed in Section 3.

2.3. *Post-bifurcation equilibrium for global critical mode—asymptotics near critical point*

The bifurcated equilibrium solution corresponding to the long wavelength mode of the perfect structure described above can be determined by the associated homogenized energy density $W^H(\lambda, \gamma)$. This is a finite quantity depending on load parameter λ and bifurcation amplitude ξ and the general LSK asymptotic theory is applicable. Hence we can characterize the stability of the principal and bifurcated paths near the critical point, show the connection with the vanishing of the homogenized tangent shear modulus and find the (asymptotic) solution when an analytical one is not possible.

The bifurcated equilibrium path of the infinite, perfect structure can be obtained from its homogenized energy density, defined by:

$$W^H(\lambda, \gamma) = \langle W \rangle \equiv \zeta_f W^f + \zeta_m W^m. \tag{2.10}$$

By extremizing the homogenized potential energy $\langle W \rangle - \Lambda\lambda$ with respect to the displacement parameters λ, γ introduced in Section 2.2, we show that the onset of bifurcation coincides with the vanishing of the homogenized moduli $L^H_{2121}(\lambda_c)$ in (2.7). Indeed, a slightly stronger result is available by showing that along the principal equilibrium path (γ=0):

$$\langle W \rangle^0_{,\gamma\gamma} = L^H_{2121}(\lambda), \tag{2.11}$$

where the 0 superscript or subscript denotes evaluation on the principal equilibrium path. Indeed from (2.10) and the definitions of the 1st Piola–Kirchhoff stress and the incremental moduli in (2.3) and (2.4) one obtains:

$$\langle W \rangle^0_{,\gamma\gamma} = \left\langle L^0_{ijkl}\left[\frac{\partial F_{ij}}{\partial \gamma}\right]_{\gamma=0}\left[\frac{\partial F_{kl}}{\partial \gamma}\right]_{\gamma=0} + \Pi^0_{ji}\left[\frac{\partial^2 F_{ij}}{\partial \gamma^2}\right]_{\gamma=0}\right\rangle. \tag{2.12}$$

Notice first that in view of the kinematics $(2.8)_1$ and $(2.8)_2$ that $\left(\partial^2 F_{11}/\partial\gamma^2\right)_{\gamma=0} = \left(\partial^2 F_{21}/\partial\gamma^2\right)_{\gamma=0} = 0$. Moreover the absence of lateral stresses $\partial W^m/\partial F^m_{22} = \partial W^f/\partial F^f_{22} = 0$ in $(2.9)_4$ and the vanishing of the average shear $\langle F_{12} \rangle$ according to $(2.8)_3$ lead to the vanishing of the $\left\langle \Pi^0_{ji}\left(\partial^2 F_{ij}/\partial\gamma^2\right)_{\gamma=0}\right\rangle$ term of $\langle W \rangle^0_{,\gamma\gamma}$ in (A.16). Consequently and since from kinematics $\partial F_{11}/\partial\gamma = 0$, $\partial F_{21}/\partial\gamma = 1$ according to $(2.8)_1$ and $(2.8)_2$ respectively, (A.16) can be rewritten as:

$$\langle W \rangle^0_{,\gamma\gamma} = \left\langle L^0_{2121} + \left(L^0_{2112} + L^0_{1221}\right)\left[\frac{\partial F_{12}}{\partial \gamma}\right]_{\gamma=0} + L^0_{1212}\left[\frac{\partial F_{12}}{\partial \gamma}\right]^2_{\gamma=0}\right\rangle. \tag{2.13}$$

In the derivation of (A.17) use is made of the fact that in view of the orthotropy of the principal solution $L^0_{1211} = L^0_{1222} = L^0_{2111} = L^0_{2122} = 0$ (plus all the principal symmetry related moduli) vanish, plus the fact $\left(\partial F_{22}/\partial\gamma\right)_{\gamma=0} = 0$, which follows from the principal solution's orthotropy and the vanishing of the lateral stress $\Pi^m_{22} = \Pi^f_{22} = 0$.

The last remaining ingredient to prove (2.11) is the calculation of $\left(\partial F_{12}/\partial\gamma\right)_{\gamma=0}$ for the matrix and fiber layers respectively. Indeed from taking the γ-derivatives of $(2.8)_3$ and $(2.9)_3$ one has:

$$\begin{aligned} &\zeta_m\left[\frac{\partial F^m_{12}}{\partial \gamma}\right]_{\gamma=0} + \zeta_f\left[\frac{\partial F^f_{12}}{\partial \gamma}\right]_{\gamma=0} = 0, \\ &L^{0m}_{1212}\left[\frac{\partial F^m_{12}}{\partial \gamma}\right]_{\gamma=0} + L^{0m}_{1221} = L^{0f}_{1212}\left[\frac{\partial F^f_{12}}{\partial \gamma}\right]_{\gamma=0} + L^{0f}_{1221}. \end{aligned} \tag{2.14}$$

From the above linear system one can calculate $\left(\partial F^m_{12}/\partial\gamma\right)_{\gamma=0}$ and $\left(\partial F^f_{12}/\partial\gamma\right)_{\gamma=0}$, which upon substitution into (A.17) and

recalling the definition of $L^H_{2121}(\lambda)$ in (A.21)$_4$, gives (2.11).

For the case of a hyperelastic layered composite of arbitrary energy density and volume fractions where a closed-form analytical solution is not possible, the initial stability of the bifurcated equilibrium path near the critical load can be found asymptotically. The bifurcation amplitude parameter of the system is the shear γ (principal solution $\gamma=0$). Due to the symmetry of the problem, one has near the critical point the following asymptotic expressions for the applied average stress (Λ) or average strain (λ):

$$\Lambda = \Lambda_c + \Lambda_2\frac{\gamma^2}{2} + O(\gamma^4), \quad \lambda = \lambda_c + \lambda_2\frac{\gamma^2}{2} + O(\gamma^4). \tag{2.15}$$

The goal of the asymptotic analysis is to obtain Λ_2 and λ_2 as functions of geometry and material properties of the composite. Consequently, according to the general theory of stability of an elastic system with a simple eigenmode at criticality (the homogenized perfect composite has a finite energy given in (2.10)), for displacement control, the stability of the bifurcated path near the critical point requires $\lambda_2 > 0$ (or equivalently $\Lambda_2 > 0$) for force control.

3. Results

Following the presentation of the constitutive laws for the composite in Section 3.1, we proceed to the general formulation of the post-bifurcated equilibrium path for infinite, incompressible, hyperelastic layered composites in Section 3.2. It is subsequently shown in Section 3.3, that all perfect neo-Hookean composites irrespectively of fiber-to-matrix thickness ratio, have an initial post-bifurcation response with increasing load and displacement. We then present in Section 3.4 a more general layered composite, consisting of an equal thickness neo-Hookean layer and a softer nonlinear matrix, that can exhibit all possible post-critical responses. It is worth noticing that all these different post-bifurcation responses can be achieved with composites made of locally stable, i.e. strongly elliptic layers. Numerical (FEM) calculations for boundary value problems showing the absence or presence of localized deformation zones in these composites, in accordance with the predicted initial post-bifurcation response of their perfect counterparts, are presented in Section 3.5.

3.1. Constitutive laws

Two different versions of a rank-one convex, plane strain, isotropic, hyperelastic constitutive law are employed. The incompressible version—used for its analytical tractability—of any isotropic hyperelastic solid subjected to plane strain can be written in terms of a one variable scalar function $g(z)$:[3]

$$W(\mathbf{F}) = \frac{\mu}{2}g(z); \quad z \equiv I_1 - 2, \quad I_2 = 1, \quad g(0) = 0, \quad g'(0) = 1, \tag{3.1}$$

where $\mu > 0$ is the initial shear modulus of the material and I_i ($i=1,2$) are the two invariants of the right Cauchy–Green tensor $\mathbf{C}$, (related to the deformation gradient tensor $\mathbf{F}$ by $C_{ij} = F_{ki}F_{kj}$), namely:

$$I_1 = \text{tr } \mathbf{C}, \quad I_2 = \frac{1}{2}\left[(\text{tr } \mathbf{C})^2 - \text{tr } \mathbf{C}^2\right] = \text{Det}(\mathbf{C}). \tag{3.2}$$

Rank-one convexity is guaranteed when $g' > 0$ and $g'' \geq 0$ (rank-one convexity requires a weaker condition: $g' + 2zg'' > 0$, since $z \geq 0$). The special case $g(z) = z$ corresponds to a *neo-Hookean* solid.

A compressible version of (3.1) will also be used:

$$W(\mathbf{F}) = \frac{\mu}{2}g(y) + \frac{\kappa}{2}(I_2^{1/2} - 1)^2; \quad y \equiv I_1 - 2I_2^{1/2}, \tag{3.3}$$

where μ and $\kappa \gg \mu$ are the initial shear and bulk moduli of the solid. This material's rank-one convexity follows from its polyconvexity (see Ball, 1977) which is guaranteed, since $y \geq 0$, by: $g' > 0$ and $g'' \geq 0$.

3.2. Post-bifurcation equilibrium—general setting

As previously mentioned, a closed-form analytical solution of the post-bifurcation equilibrium path described in Section 2.2. is not in general possible, thus motivating the need for the asymptotic analysis presented in Section 2.3. However, for the special case of incompressibility or of the case of compressible neo-Hookean composites one can find analytically tractable expressions for the post-bifurcation equilibrium paths.

For the incompressible composite in (3.1), the constitutive law of (2.3) takes the form:

[3] Here and subsequently g', g'' etc. denote the first and second derivatives of g with respect to its argument.

$$\Pi_{ji} = \frac{\partial W}{F_{ij}} - p\,\frac{\partial}{\partial F_{ij}}(\det(\mathbf{F}) - 1),$$
$$\det(\mathbf{F}) = (I_2)^{1/2} = F_{11}\,F_{22} - F_{12}\,F_{21} = 1, \tag{3.4}$$

where p is the Lagrange multiplier associated to the incompressibility constraint (the undefined part of the hydrostatic pressure).

Recalling from the kinematics in (2.8)$_1$, (2.8)$_2$ that $F_{11} = 1 - \lambda$ and $F_{21} = \gamma$ one obtains that:

$$\Pi_{11} = \mu\, g'\left[1 - \lambda - \frac{(1+\gamma F_{12})^2}{(1-\lambda)^3}\right],$$
$$\Pi_{22} = 0 \quad \Rightarrow \quad p = \mu\, g'\,\frac{(1+\gamma F_{12})}{(1-\lambda)^2},$$
$$\Pi_{21} = \mu\, g'\left[F_{12} + \gamma\frac{(1+\gamma F_{12})}{(1-\lambda)^2}\right],$$
$$\Pi_{12} = \mu\, g'\left[\gamma + \frac{F_{12}(1+\gamma F_{12})}{(1-\lambda)^2}\right]. \tag{3.5}$$

From shear traction continuity $\Pi_{21}^f = \Pi_{21}^m$ from (2.9)$_3$ and the kinematic constraint that $\langle F_{12}\rangle = 0$ from (2.8)$_3$ one has the following system for the two unknowns F_{12}^f and F_{12}^m:

$$\left[1 + \frac{\gamma^2}{(1-\lambda)^2}\right]\left[m_f\,F_{12}^f - m_m\,F_{12}^m\right] + \frac{\gamma}{(1-\lambda)^2}(m_f - m_m) = 0,$$
$$\zeta_f\,F_{12}^f + \zeta_m\,F_{12}^m = 0,$$
$$m_f \equiv \mu_f\, g_f', \quad m_m \equiv \mu_m\, g_m'. \tag{3.6}$$

Solving the above linear system for F_{12}^f, F_{12}^m yields:

$$F_{12}^f = \frac{\gamma}{(1-\lambda)^2 + \gamma^2}\,\frac{(m_m - m_f)\zeta_m}{\zeta_f\,m_m + \zeta_m\,m_f},$$
$$F_{12}^m = \frac{\gamma}{(1-\lambda)^2 + \gamma^2}\,\frac{(m_f - m_m)\zeta_f}{\zeta_f\,m_m + \zeta_m\,m_f}. \tag{3.7}$$

The λ–γ relationship along the bifurcated equilibrium path can now be obtained by combining $\langle \Pi_{12}\rangle = 0$ from (2.9)$_2$ with the expressions for $\Pi_{12}^{f,m}$ and $F_{12}^{f,m}$ in (3.5)$_4$ and (3.7):

$$\langle \Pi_{12}\rangle = \gamma\left\{m_G - \frac{(\Delta m)^2}{m_H}\,\frac{1}{\left[(1-\lambda)^2 + \gamma^2\right]^2}\right\},$$
$$\Delta m \equiv m_f - m_m, \quad m_G \equiv \zeta_f\,m_f + \zeta_m\,m_m, \quad m_H \equiv \frac{m_f}{\zeta_f} + \frac{m_m}{\zeta_m}. \tag{3.8}$$

Thus the sought λ–γ relationship takes the form:

$$(1-\lambda)^2 + \gamma^2 = \frac{\Delta m}{(m_G\,m_H)^{1/2}}, \tag{3.9}$$

where without loss of generality we have tacitly assumed $\Delta m > 0$ i.e. that $m_f > m_m$.

One important remark about (3.9) is in order at this point, namely that this is an implicit equation for λ and γ, given the fact that m_f and m_m are functions of I_1^f and I_1^m which in turn depend on λ and γ by:

$$I_1 = F_{ij}F_{ij} = (1-\lambda)^2 + \left(\frac{1+\gamma F_{12}}{1-\lambda}\right)^2 + (F_{12})^2 + \gamma^2, \tag{3.10}$$

where the expressions for F_{12} in the fiber and matrix layers are given in (3.7). The critical axial strain λ_c is found from (3.9) for γ=0.

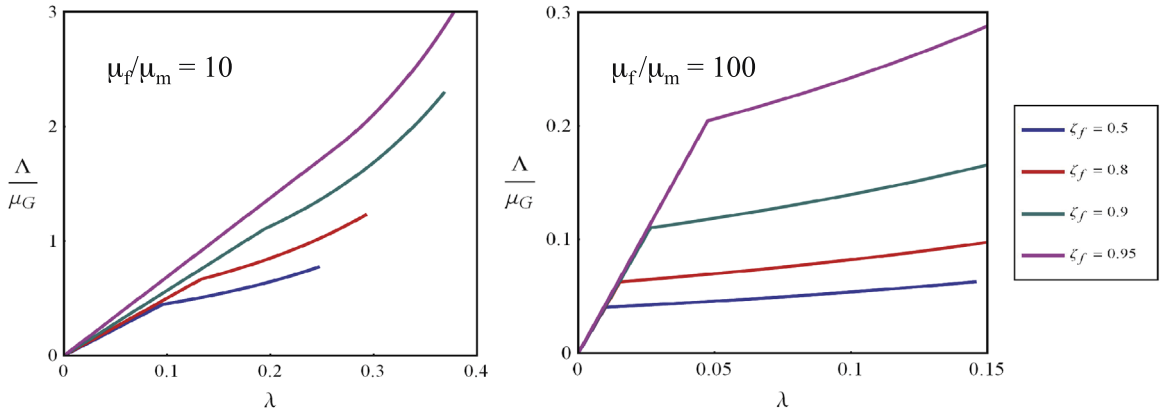

Fig. 5. Dimensionless macroscopic axial stress Λ/μ_G vs. its work-conjugate strain λ for the principal and bifurcated equilibrium path of perfect neo-Hookean composites with $\mu_f/\mu_m = 10$ (left) and $\mu_f/\mu_m = 100$ (right) calculated for four different volume fractions.

3.3. Neo-Hookean composites

As it turns out, the simplest case of a neo-Hookean composite (where $g(z) = z$) is always stable under either force of displacement control with monotonically increasing forces and displacements as functions of the shear γ. Moreover, a closed-form solution is possible in this case, since $m_f = \mu_f$ and $m_m = \mu_m$ are now constants:

$$(1-\lambda)^2 + \gamma^2 = \frac{\Delta\mu}{(\mu_G\,\mu_H)^{1/2}} \quad \Longrightarrow \quad \lambda = 1 - \left[\frac{\Delta\mu}{(\mu_G\,\mu_H)^{1/2}} - \gamma^2\right]^{1/2},$$
$$\Delta\mu \equiv \mu_f - \mu_m, \quad \mu_G \equiv \zeta_f\,\mu_f + \zeta_m\,\mu_m, \quad \mu_H \equiv \left(\frac{\mu_f}{\zeta_f}\right) + \left(\frac{\mu_m}{\zeta_m}\right), \tag{3.11}$$

where it is tacitly assumed that the shear strain satisfies: $0 \le \gamma < (\Delta\mu)^{1/2}/(\mu_G\,\mu_H)^{1/4}$.

Using (3.11), we calculate Λ, the absolute value of the average compressive stress $\langle \Pi_{11} \rangle$:

$$\Lambda = -\langle \Pi_{11} \rangle = \frac{\mu_G}{(1-\lambda)^3}\{1 - \left[(1-\lambda)^2 + \gamma^2\right]^2\} = \mu_G\left[\frac{1 - \dfrac{(\Delta\mu)^2}{(\mu_G\,\mu_H)}}{\left(\dfrac{\Delta\mu}{(\mu_G\,\mu_H)^{1/2}} - \gamma^2\right)^{3/2}}\right]. \tag{3.12}$$

The absolute value of the dimensionless axial stress Λ/μ_G vs. its work-conjugate strain λ is depicted in Fig. 5, which shows that the stable equilibrium paths of four different volume fraction neo-Hookean composites for two different values of fiber-to-matrix stiffness ratios $\mu_f/\mu_m = 10,\ 100$. The corresponding stress–strain relations are:

$$\text{principal: } \Lambda = \frac{\mu_G}{(1-\lambda)^3}[(1-\lambda)^4 - 1]\ 0 \le \lambda \le \lambda_c; \quad \text{bifurcated: } \Lambda = \frac{\mu_G}{(1-\lambda)^3}\left[1 - \frac{(\Delta\mu)^2}{\mu_G\,\mu_H}\right] 1 > \lambda \ge \lambda_c. \tag{3.13}$$

As expected, increasing the fiber-to-matrix stiffness ratio, leads to a sharp decrease in the slope of the bifurcated equilibrium path, in view of an increasingly softening matrix response in the post-bifurcated path. From (3.11) one obtains, by setting γ=0, the following simple expression for the critical load λ_c under displacement control for the neo-Hookean composite:

$$\lambda_c = 1 - \left(\frac{(\Delta\mu)^2}{\mu_G\,\mu_H}\right)^{1/4}. \tag{3.14}$$

The influence of fiber volume fraction and stiffness contrast on the critical strain λ_c is depicted in Fig. 6. The reference critical strain λ_{ref} used for calculating the influence of fiber volume fraction under fixed stiffness contrast corresponds to $\zeta_f = 0.5$ (and changes according to the stiffness contrast), while the reference critical strain λ_{ref} used for calculating the influence of stiffness contrast under fixed fiber volume fraction corresponds to $\mu_f/\mu_m = 2$ (and changes according to the fiber volume fraction). As expected the critical strain increases monotonically with increasing fiber volume fraction, while for a fixed fiber volume fraction, the critical strain decreases monotonically with increasing fiber-to-matrix stiffness ratio.

The influence of fiber volume fraction and stiffness contrast on the critical stress Λ_c is depicted in Fig. 7. The reference critical stress Λ_{ref} used for calculating the influence of fiber volume fraction under fixed stiffness contrast corresponds to

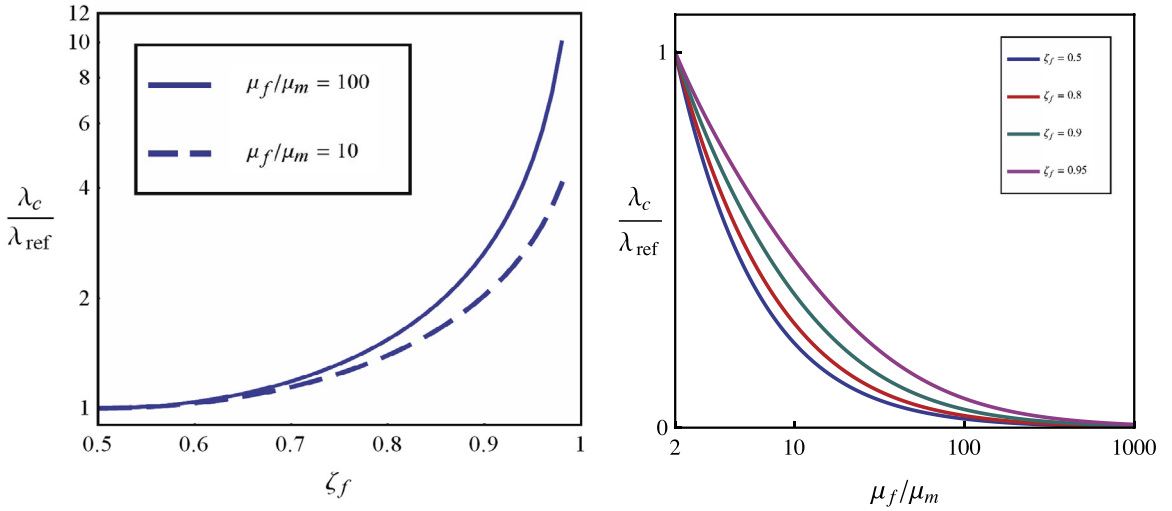

Fig. 6. Influence of fiber volume fraction on the critical strain for two different fiber-to-matrix stiffness ratios (left) and influence of the fiber-to-matrix stiffness contrast on the critical strain for four different volume fractions (right).

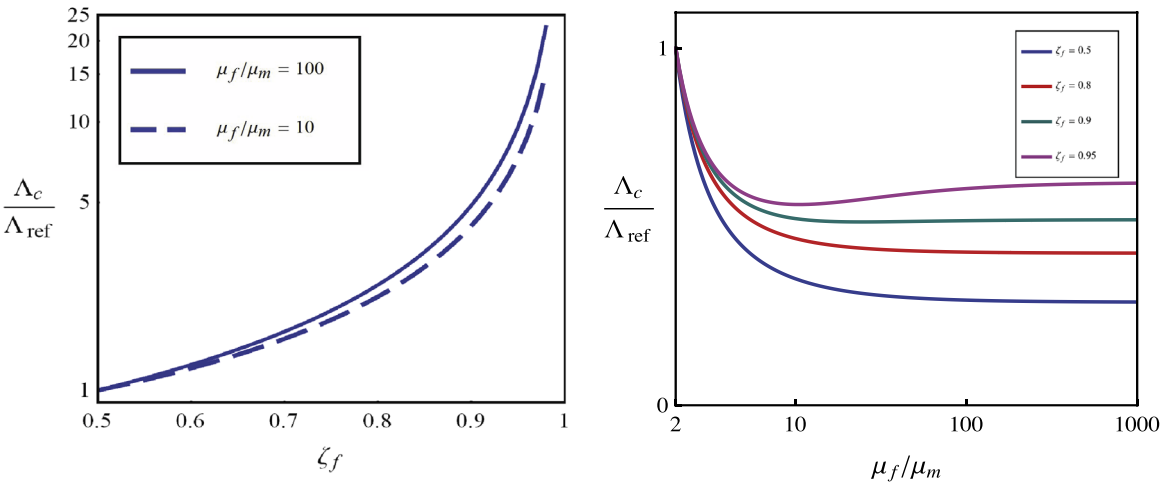

Fig. 7. Influence of fiber volume fraction on the critical stress for two different fiber-to-matrix stiffness ratios (left) and influence of the fiber-to-matrix stiffness contrast on the critical stress for four different volume fractions (right).

$\zeta_f = 0.5$ (and changes according to the stiffness contrast), while the reference critical stress Λ_{ref} used for calculating the influence of stiffness contrast under fixed fiber volume fraction corresponds to $\mu_f/\mu_m = 2$ (and changes according to the fiber volume fraction). As expected the critical stress increases monotonically with increasing fiber volume fraction, while for a fixed fiber volume fraction, the critical stress after a steep initial decrease with increasing fiber-to-matrix stiffness ratio, reaches a plateau after about $\mu_f/\mu_m = 10$ but not in a monotonic fashion, as seen in particular for $\zeta_f = 0.95$.

Since an analytical expression is available for the entire homogenized, post-bifurcated equilibrium path in a perfect neo-Hookean composite according to (3.11) and (3.12), one can find the stability of this equilibrium path by checking the positive definiteness of the homogenized energy. For algebraic simplicity, we calculate here the initial curvatures at criticality λ_2 and Λ_2, whose positivity implies stability, according to the general theory, at least in a neighborhood of the critical point.

At criticality, the strain curvature λ_2 of the neo-Hookean composite's bifurcated equilibrium path is found from (3.11):

$$\lambda_2 = \frac{1}{1-\lambda_c} \implies \frac{\lambda_2}{\lambda_c} = \frac{1}{\lambda_c(1-\lambda_c)} \tag{3.15}$$

The corresponding curvature Λ_2 is obtained by evaluating $\left(d^2\Lambda/d\gamma^2\right)_{\gamma=0}$ from (3.12):

$$\Lambda_2 = \frac{3\,\mu_G}{1-\lambda_c}\left[\frac{1}{(1-\lambda_c)^4} - 1\right] \implies \frac{\Lambda_2}{\Lambda_c} = \frac{3}{(1-\lambda_c)^2}. \tag{3.16}$$

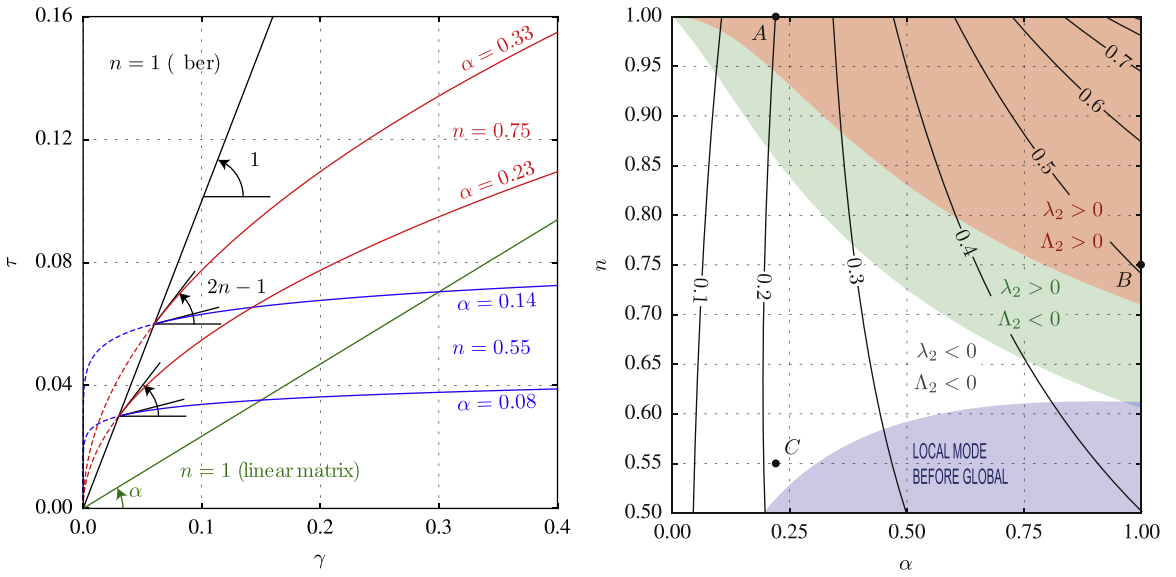

Fig. 8. Left: Uniaxial response in simple shear ($\tau - \gamma$) of the neo-Hookean fiber (linear, in black) and of the matrix (in color, for different values of the hardening exponent n) of a composite containing two equal thickness layers. Right: Initial post-bifurcation stability behavior of this composite at a given critical load (λ_c, in solid black lines) as a function of matrix constitutive parameters α, n. Area shaded red: $\Lambda_2 > 0$, $\lambda_2 > 0$, area shaded green: $\Lambda_2 < 0$, $\lambda_2 > 0$, remaining non-shaded area: $\Lambda_2 < 0$, $\lambda_2 < 0$. The blue shaded area at the bottom of the graph indicates composites where a local bucking mode precedes the global one. (For interpretation of the references to color in this figure caption, the reader is referred to the web version of this paper.)

We have thus shown that for the perfect, incompressible neo-Hookean composite, its homogenized post-bifurcation path has monotonically increasing displacements and forces; it is thus stable near the critical point and even beyond.

This result is not surprising; in contrast to classical fiber reinforced composites where the much stiffer fiber is linearly elastic while the soft matrix has a low hardening which favors shearing of the matrix and unloading of the fiber leading to a decreasing displacement (snap-back), here each layer of the composite stiffens at the same rate, resulting in an increasing force and displacement at the bifurcated equilibrium path.

It is worth checking if this strong post-bifurcation stability result found for arbitrary neo-Hookean composites is influenced by compressibility; it turns out that it is not and the corresponding calculations are in Appendix B.

3.4. *Rank-one convex composites exhibiting all possible cases of post-bifurcation response*

We have proved that the homogenized, post-bifurcation equilibrium path of a perfect layered composite consisting of two neo-Hookean layers of arbitrary shear moduli and volume fractions is stable (near the critical load), under either force ($\Lambda_2 > 0$) or displacement ($\lambda_2 > 0$) control. An even stronger result holds: the homogenized, post-bifurcation equilibrium paths of the perfect neo-Hookean composite have a monotonically increasing macroscopic stress and strain as the bifurcation amplitude γ increases ($d\Lambda/d\gamma > 0$ and $d\lambda/d\gamma > 0$), as one can easily show from (3.11) and (3.12).

The question that naturally arises is whether a different choice of a locally stable (i.e. rank-one convex) constitutive laws, i.e. a nonlinear $g(z)$ in (3.1), can lead to an unstable post-bifurcation response. The answer to this question is affirmative and we present below composites that exhibit unstable post-bifurcated equilibrium paths even under displacement control, i.e. $\lambda_2 < 0$.

For analytical tractability, we consider composites of two equal thickness layers ($\zeta_f = \zeta_m = 0.5$) but different energy densities, defined by (3.1):

$$g_f(z) = \frac{1}{2}z, \quad g_m(z) = \frac{\alpha}{2}z^n; \quad 1 \geq \alpha > 0, \quad 1 \geq n > 0.5. \tag{3.17}$$

Since the material is isotropic, incompressible and under plane strain conditions, it is best described by its response in simple shear γ. Recalling that under simple shear $(\gamma)^2 = z$ ($\equiv I_1 - 2$) and that its shear stress $\tau = dW/d\gamma$, we record in Fig. 8 the response of the fiber and matrix layers. The response of the neo-Hookean fiber is linear ($\mu_f = 1$) and always stiffer than the response of the matrix, which exhibits softening under increasing applied strain. The singularity of the matrix material at the origin can be removed[4] and the shear strain γ_m where the matrix response starts differing from the fiber's is adjusted

[4] We set $g_f(z) = g_m(z)$ for $0 \leq z \leq z_m$ and $g_m(z) = 0.5\alpha z^n$ for $z \geq z_m$, where $z_m = (\gamma_m)^2$ with γ_m the shear strain that marks the onset of the matrix nonlinear response. Continuity of shear stress at γ_m dictates that: $n\alpha = z_m^{(1-n)}$. Note that the matrix material is always strongly rank-one convex since $d^2W/d\gamma^2 > 0$.

by the parameter α as seen in Fig. 8. The equal layer thickness neo-Hookean composite is recovered for a matrix with $n=1$ and $\alpha = \mu_m/\mu_f$.

For the case $\zeta_f = \zeta_m = 0.5$ one obtains from (3.7):

$$F_{12}^f = -\gamma, \quad F_{12}^m = \gamma, \tag{3.18}$$

thus yielding with the help of (3.10) the following expressions for the strain invariant I_1 in each layer:

$$I_1^f = (1-\lambda)^2 + \frac{1}{(1-\lambda)^2} + 2\gamma^2\left[1 - \frac{1}{(1-\lambda)^2}\right] + \frac{\gamma^4}{(1-\lambda)^2} = z_f + 2,$$
$$I_1^m = (1-\lambda)^2 + \frac{1}{(1-\lambda)^2} + 2\gamma^2\left[1 + \frac{1}{(1-\lambda)^2}\right] + \frac{\gamma^4}{(1-\lambda)^2} = z_m + 2. \tag{3.19}$$

Consequently the λ - γ relationship along the bifurcated equilibrium path in (3.9) takes the form (after recalling also the definitions for m_f, m_m in $(3.6)_3$):

$$(1-\lambda)^2 + \gamma^2 = \frac{1 - n\alpha(z_m)^{n-1}}{1 + n\alpha(z_m)^{n-1}}. \tag{3.20}$$

The corresponding expression for the macroscopic stress along the bifurcated equilibrium path is found to be:

$$\Lambda = -\langle \Pi_{11}\rangle = \frac{1 + n\alpha(z_m)^{n-1}}{2(1-\lambda)^3}\left\{1 - \left[(1-\lambda)^2 + \gamma^2\right]^2\right\}. \tag{3.21}$$

Solving Eq. (3.20) for $\gamma=0$ yields the following implicit equation for the critical strain λ_c:

$$n\alpha\left[(1-\lambda_c)^2 + \frac{1}{(1-\lambda_c)^2} - 2\right]^{(n-1)} = \frac{1-(1-\lambda_c)^2}{1+(1-\lambda_c)^2}, \tag{3.22}$$

where the bifurcation occurs at the lowest positive root λ_c of the implicit equation (3.22).

Of interest is the initial post-bifurcation behavior of this composite, i.e. the curvatures λ_2 and Λ_2 of the bifurcated equilibrium path at critical load. To this end, by taking into account (3.19), we differentiate (3.20) with respect to γ at $\gamma=0$ to find:

$$\lambda_2 = \frac{(1-\lambda_c)}{1-(1-\lambda_c)^2}\left[\frac{1-(1-\lambda_c)^2 - (1-n)\left[1+(1-\lambda_c)^2\right]^2}{(1-\lambda_c)^2 + \frac{1-n}{2}\left[1+(1-\lambda_c)^2\right]^2}\right]. \tag{3.23}$$

Initial post-bifurcation stability of this composite under displacement control requires $\lambda_2 > 0$, i.e. that the numerator in the above expression for λ_2 be positive:

$$1 - (1-\lambda_c)^2 - (1-n)\left[1+(1-\lambda_c)^2\right]^2 > 0. \tag{3.24}$$

To find the initial stability under force control, by taking into account (3.22), we differentiate (3.21) with respect to γ at $\gamma=0$ to find Λ_2:

$$\Lambda_2 = \frac{(1-\lambda_c)^{-3}}{1-(1-\lambda_c)^2}\left[\frac{3\left[1-(1-\lambda_c)^2\right]^2 - 2(1-n)\left[2-(1-\lambda_c)^2\right]\left[1+(1-\lambda_c)^2\right]^2}{(1-\lambda_c)^2 + \frac{1-n}{2}\left[1+(1-\lambda_c)^2\right]^2}\right]. \tag{3.25}$$

Initial post-bifurcation stability of this composite under force control requires $\Lambda_2 > 0$, i.e. that the numerator in the above expression for Λ_2 be positive:

$$3\left[1-(1-\lambda_c)^2\right]^2 - 2(1-n)\left[2-(1-\lambda_c)^2\right]\left[1+(1-\lambda_c)^2\right]^2 > 0. \tag{3.26}$$

The range of matrix constitutive parameters (α, n, see definition in (3.17)), for which the homogenized, post-bifurcated solution is initially stable under either force or displacement control ($\Lambda_2 > 0$, $\lambda_2 > 0$, red-shaded area), is initially stable only under displacement control ($\Lambda_2 < 0$, $\lambda_2 > 0$, green-shaded area) and initially unstable under either force or displacement control ($\Lambda_2 < 0$, $\lambda_2 < 0$, non-shaded area), is given in Fig. 8. The same figure also records contours of equal critical strain λ_c as a function of the matrix constitutive parameters α, n. Notice that for large critical strains (approximately $\lambda_c > 0.5$) the composite is initially stable, while for small strains (depending on the value of n) the composite exhibits a snap-back ($\lambda_2 < 0$). A word of caution: for the post-bifurcation results to be meaningful, one should select matrix parameters α, n for which the critical mode is global in nature, i.e. exclude composites with matrix parameters in the blue-shaded area of Fig. 8 (see discussion in Section 2). The results obtained in Fig. 8 are important in selecting composites for the numerical calculations of the boundary value problems reported in the next section.

3.5. Boundary value problem calculations

Thus far we have established the homogenized post-bifurcation behavior of an infinite, perfect, fiber-reinforced, hyperelastic composite compressed axially along the direction of its fibers. We want to find out the response in the bulk of such a composite (i.e. away from boundaries) by solving an appropriate boundary value problem, in order to establish whether a localized pattern of deformation will actually emerge or not, once the critical load is approached, given that the energy density of the homogenized principal solution loses its rank-one convexity once a critical macroscopic strain (λ_c) or stress (Λ_c) has been reached. We seek the equilibrium path of a *"realistic"* such composite, i.e. one with the inevitable small imperfections and finite boundaries; in the interest of avoiding edge effects, an adequately large sample should be considered and the perturbation should vanish on the sample edges. No analytical solution being possible (to the best of our knowledge) for a finite size, imperfect composite, a numerical one is sought based on FEM discretization of the corresponding boundary value problem. It should be mentioned at this point that there is a vast amount of work dedicated to the problem of multiscale calculations, i.e. how to find the response of a microstructured solid which is prone to localization by selecting an appropriate representative volume element, consistent boundary conditions and an efficient computational strategy. Our main concern for the FEM calculations is the avoidance of boundary strain concentrations and this is achieved by the procedure described below. However, the reader interested in this aspect of the problem is referred to the recent article by Coenen et al. (2012), who propose an interesting computational strategy for arbitrary microstructures and also present a very comprehensive literature review.

To this end we seek the solution of a finite-size, initially square segment of the composite (of dimensions $L \times L$), subjected to a macroscopic (average) deformation gradient with $\langle F_{11}\rangle = 1-\lambda$, $\langle F_{12}\rangle = 0$ and a macroscopic (average) first Piola–Kirchhoff stress with $\langle \Pi_{12}\rangle = \langle \Pi_{22}\rangle = 0$, in agreement with (2.8) and (2.9). Moreover, periodic boundary conditions are imposed on opposite faces of this square segment, so that the perfect, finite-size composite can exhibit both the perfect principal and perfect bifurcated solutions presented in Section 2.2, thus avoiding the development of large deviations from the perfect solution at the boundaries.

Several such finite-size composites are investigated; the results presented here correspond to an initially square segment containing 40 unit cells, with each such cell consisting of a fiber layer (initial dimension $L/80 \times L$ and a matrix layer (initial dimension $L/80 \times L$; only composites with equal matrix and fiber volume fractions ($\zeta_m = \zeta_f = 0.5$) are modeled. Each fiber and matrix layer are discretized using a Cartesian grid of 4 quadrilateral elements through the thickness and 320 elements along their length for a grid consisting of a total of 102,400 such elements. The FEM calculations are performed using ABAQUS by implementing the constitutive relations in (3.17) into the incompressible element CPE4H.

The reference configuration of the sample has a small geometric imperfection with respect to its perfect counterpart, which is necessary to trigger the bifurcated solution. Accordingly the following initial imperfection which is designed to have a maximum amplitude at the middle of the finite-size composite and vanish at its boundaries:

$$\Delta X_1 = 0, \quad \Delta X_2 = \xi \sin(\pi X_2/L)\arctan[\beta(X_1/L - 1/2)], \tag{3.27}$$

where the parameter $\xi = 10^{-3}$ controls the maximum X_2-amplitude of the perturbation and the parameter $\beta = 8$ controls its X_1-range. The origin of the coordinate system is taken at the bottom left corner of the domain. The control parameter is the macroscopic axial strain λ and a Riks continuation method is employed to bypass the limit loads which are associated to snapbacks.

The FEM calculations presented correspond to three different composites, described in Section 3.4; the material parameters of their matrix layers are indicated by a dot in Fig. 8, which gives the initial post-bifurcation of the homogenized response for the corresponding perfect composite (the $n=1$ axis corresponds to the fully neo-Hookean composite with $\alpha = \mu_m/\mu_f$, as described in Section 3.3).

The response of a neo-Hookean composite with $\zeta_f = \zeta_m = 0.5$ and $\alpha = \mu_m/\mu_f = 0.22$, whose perfect configuration exhibits a stable post-bifurcation behavior ($\Lambda_2 > 0$, $\lambda_2 > 0$), is shown in Fig. 9. The composite has two equal thickness neo-Hookean ($n=1$) layers (see point A in Fig. 8). On the left is the macroscopic stress–strain response of the homogenized perfect composite (in red) and of its finite size imperfect counterpart, based on FEM computations using 40 unit cells (in black). In the middle and on the right are depicted the deformed configurations at points a and b, showing also contours of the Lagrangian shear strain component E_{12}. The macroscopic stress–strain curve of the imperfect composite is almost indistinguishable from its perfect counterpart. When the critical strain λ_c is reached at point a, the imperfect composite shows a higher strain zone in the middle, as seen in the middle picture of Fig. 9. Upon further increase of the applied macroscopic strain, the composite reaches at point b a uniform solution corresponding to the bifurcated state of its perfect counterpart, as shown in the right picture of Fig. 9. In contrast to what is known in typical engineering composites, the present example shows a case where in spite of losing its macroscopic rank-one convexity, the composite exhibits no localized zone of deformation in its post-critical response.

The response of a locally stable (i.e. locally rank-one convex) $\zeta_f = \zeta_m = 0.5$ composite which has a neo-Hookean fiber and a nonlinear matrix with $n = 0.75$, $\alpha = 1.0$, whose perfect configuration exhibits an initially stable post-bifurcation behavior ($\Lambda_2 > 0$, $\lambda_2 > 0$ and identified by point B in Fig. 8), is shown in Fig. 10. To the left is the macroscopic stress–strain response of the homogenized perfect composite (in red) and of its finite size imperfect counterpart based on FEM computations using 40 unit cells (in black). In the middle and on the right are depicted the deformed configurations at points a and b, showing

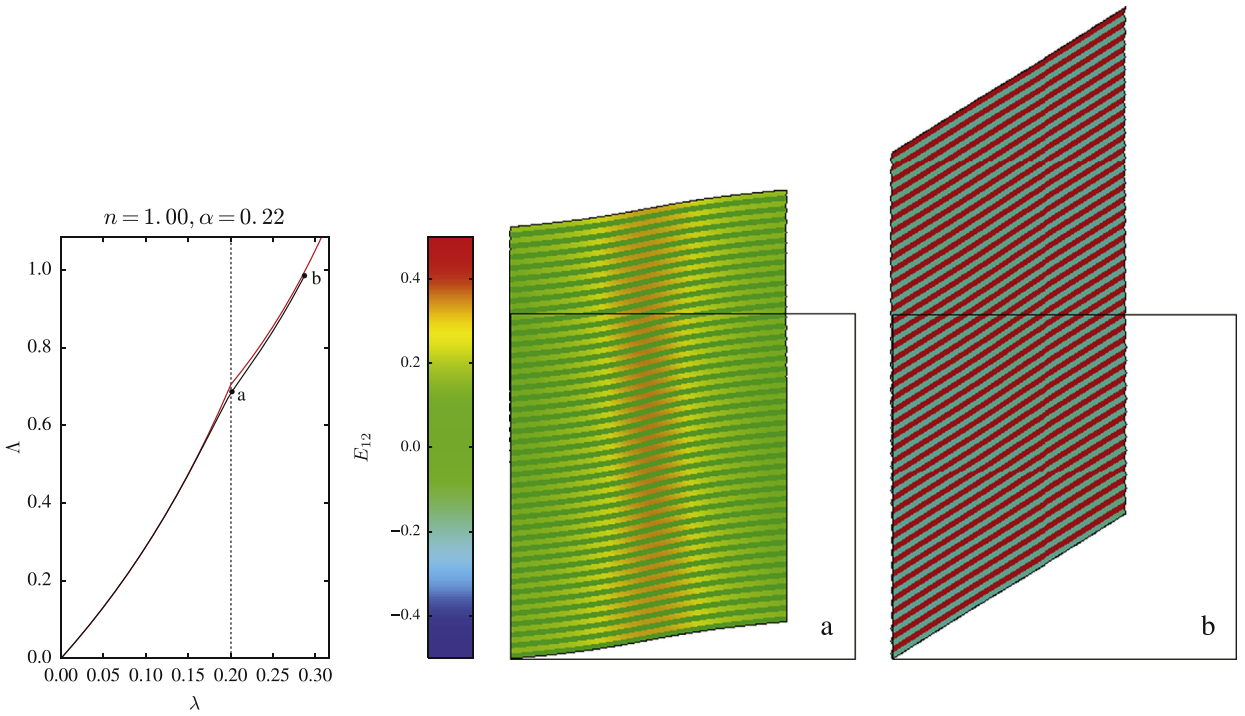

Fig. 9. Response of a neo-Hookean composite, exhibiting a stable homogenized post-bifurcation behavior ($\Lambda_2 > 0,\ \lambda_2 > 0$). The composite consists of two equal thickness neo-Hookean ($n=1$) layers with a stiffness ratio $\alpha = \mu_m/\mu_f = 0.22$, see point A in Fig. 8. On the left is the macroscopic stress–strain response of the homogenized perfect composite (in red) and of its finite size imperfect counterpart computed by FEM (in black). On the middle and right are deformed configurations at points a and b, showing also contours of the Lagrangian shear strain component E_{12}. Undeformed configuration is shown by its bounding square. (For interpretation of the references to color in this figure caption, the reader is referred to the web version of this paper.)

also contours of the Lagrangian shear strain component E_{12}. Similarly to the neo-Hookean case presented in Fig. 9, the macroscopic stress–strain curve of the imperfect composite is almost indistinguishable from its perfect counterpart. When the critical strain λ_c is reached at point a, the imperfect composite is covered by alternating higher and lower strain zones (a mix of principal and bifurcated solutions of the corresponding infinite, perfect composite), as shown in the middle picture of Fig. 10. Upon further increase of the applied macroscopic strain, the composite reaches at point b a uniform solution corresponding to the bifurcated state of the perfect composite, as seen in the right picture of Fig. 10.

The response of a locally stable (i.e. locally rank-one convex) composite with a neo-Hookean fiber and a matrix with $n = 0.55,\ \alpha = 0.22$, whose perfect configuration exhibits a homogenized post-bifurcation behavior with an initial snap-back ($\Lambda_2 < 0,\ \lambda_2 < 0$ and identified by point C in Fig. 8), is shown in Fig. 11. To the left is the macroscopic stress–strain response of the homogenized perfect composite (in red) and of its finite size imperfect counterpart based on FEM computations using 40 unit cells (in black). Due to structural effects, the post-bifurcation snap-back of the imperfect, finite-sized composite is significantly more severe than the one of its homogenized, perfect counterpart, resulting in a reversal of the macroscopic stress–strain path. It is practically impossible to distinguish in Fig. 11 between the forward loading path, which ends at point a (maximum macroscopic strain and stress) and the return path, which ends at b. The corresponding deformed configurations at points a and b, as well as the contours of the Lagrangian shear strain component E_{12} are depicted in the middle and on the right of Fig. 11.

When the maximum macroscopic strain and stress is reached (point a) one can see in the middle picture of Fig. 11 the beginning of the formation of a localized deformation zone at the middle of the imperfect composite, where the amplitude of the imperfection is maximized. When the structure has snapped back and reached point b, one can see in the right picture of Fig. 11 a very pronounced localized deformation zone, while the rest of the composite relaxes and tries to return to its principal equilibrium path. This behavior is also typical in many elastoplastic composites studied in the literature, where the localization of deformation mechanism and details of the kink band formation have been studied in detail.

All the above calculations pertain to locally stable (i.e. locally rank-one convex) hyperelastic composites that share the same feature: a critical (i.e. occurring at lowest applied macroscopic load) long wavelength bifurcation mode which corresponds to a loss of ellipticity in the homogenized principal solution. Our calculations show that a localization of deformation in these composites does not always appear in the neighborhood of critical load and beyond; the result depends on the post-bifurcation behavior of the homogenized, perfect composite. In contrast to the widely studied cases of elastoplastic composites, with high stiffness contrast between fiber and matrix that exhibit kink-band solutions, we have shown

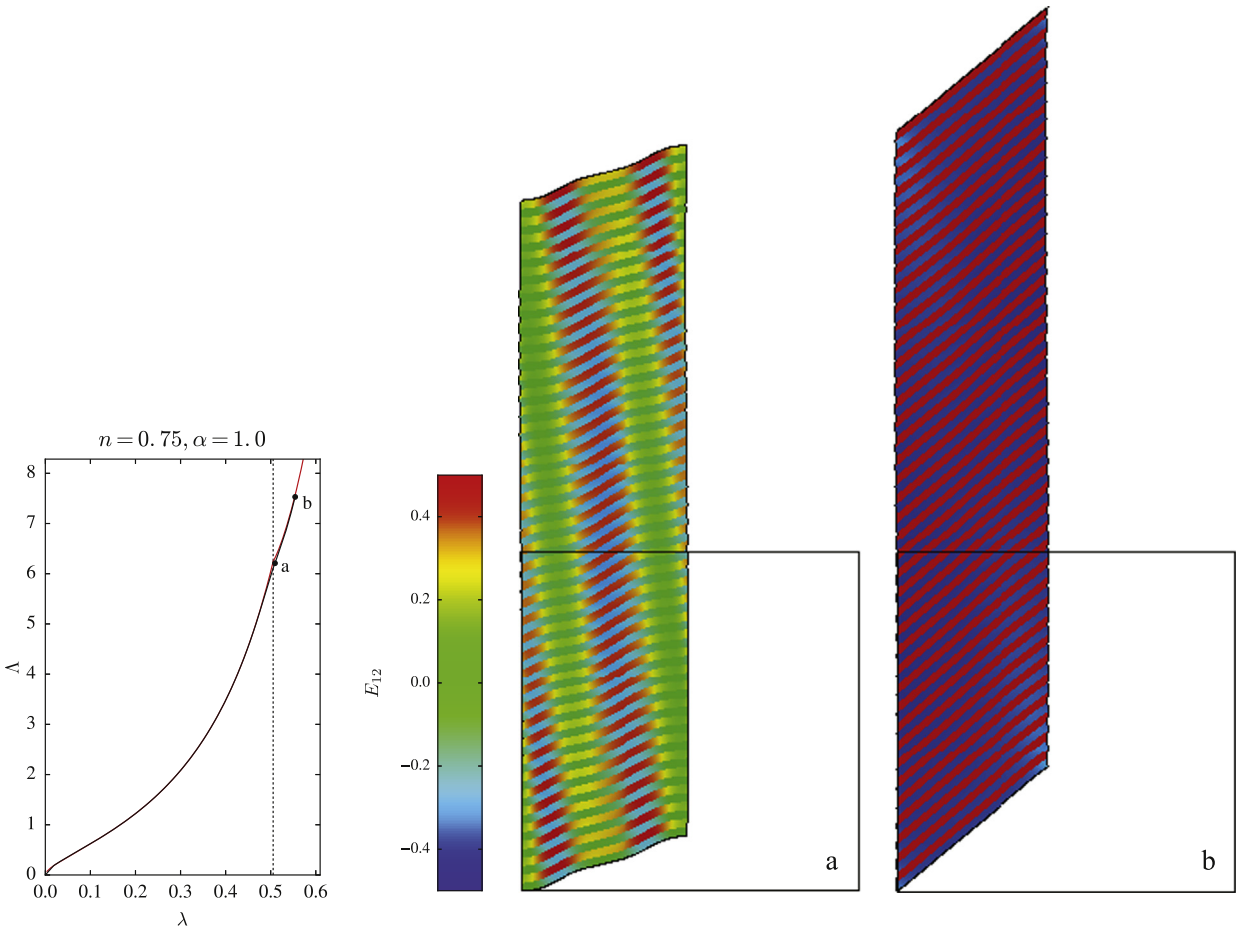

Fig. 10. Response of a composite with a stable homogenized post-bifurcation behavior $\Lambda_2 > 0$, $\lambda_2 > 0$. The composite consists of two equal thickness layers: a neo-Hookean ($n=1$) and a softer layer ($n = 0.75$, $\alpha = 1.0$, see point B in Fig. 8). On the left is the macroscopic stress–strain response of the homogenized perfect composite (in red) and of its finite size imperfect counterpart computed by FEM (in black). On the middle and right are depicted the deformed configurations at points a and b, showing also contours of the Lagrangian shear strain component E_{12}. Undeformed configuration is shown by its bounding square. (For interpretation of the references to color in this figure caption, the reader is referred to the web version of this paper.)

here the existence of composites that have stable, homogenized post-bifurcated solutions with increasing macroscopic stresses and strains. These composites do not exhibit localized deformation post-bifurcated solutions, in spite of the fact that their homogenized energy loses its rank-one convexity as the applied loading increases.

4. Conclusion

Localization of deformation in solids is the instability mechanism leading to failure by rupture. In the framework of continuum modeling, this phenomenon is captured by the loss of ellipticity in the governing equations, may lead to discontinuous strain solutions. To better understand the origins of continuum models that exhibit loss of ellipticity at adequate levels of strain or stress, a substantial amount of work has been dedicated to the nonlinear homogenization of microstructured solids to study how geometry and constitutive laws at the microscopic level lead to a macroscopic loss of ellipticity. Since a loss of ellipticity is the property allowing for discontinuous equilibrium solutions, it is thought that a loss of macroscopic (homogenized) ellipticity results in a localized deformation pattern in the post-bifurcated regime. Although this is the case in many engineering applications, it raises an interesting question: is there always a localized deformation appearing in the post-critical equilibrium path of solids loosing macroscopic ellipticity and what are the sufficient conditions in the homogenized response that lead to localization?

The present work answers these questions in the framework of a simple, but analytically tractable microstructure, namely an infinite, layered, locally stable (i.e. point-wise rank-one convex) nonlinear (hyperelastic) solid under plane strain loading conditions and more specifically under axial compression along the lamination direction. For this problem, based on a periodic unit cell construction, one can find macroscopic loads where the moduli of the homogenized principal solution loose ellipticity (and since the solid has an energy density, the corresponding homogenized energy loses rank-one

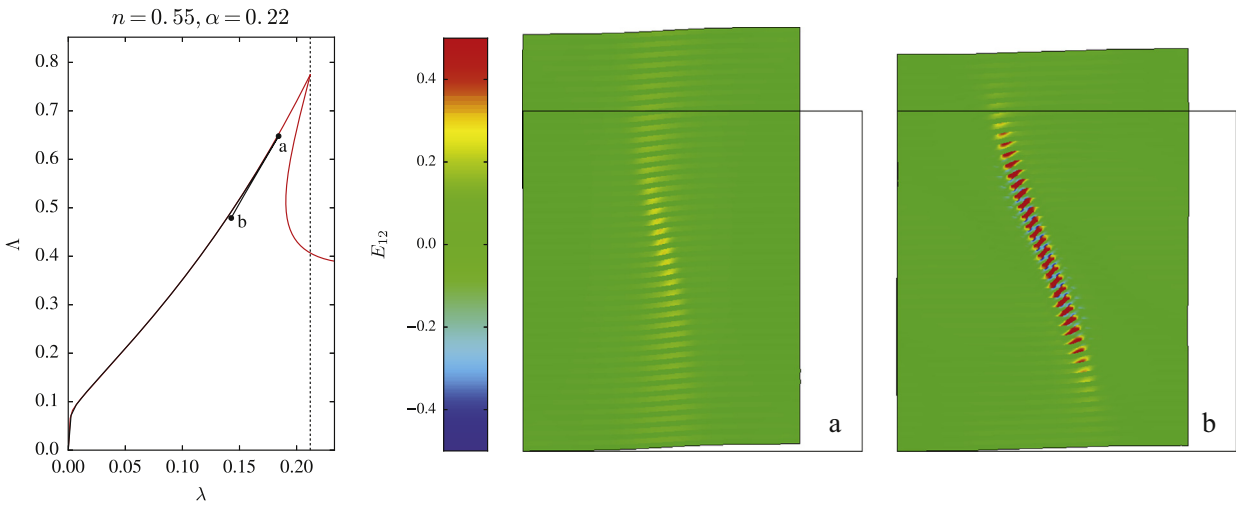

Fig. 11. Response of a composite with a snap-back homogenized initial post-bifurcation behavior $\Lambda_2 < 0,\ \lambda_2 < 0$. The composite consists of two equal thickness layers: a neo-Hookean ($n=1$) and a softer layer ($n = 0.55,\ \alpha = 0.22$, see point C in Fig. 8). On the left is the macroscopic stress–strain response of the homogenized perfect composite (in red) and of its finite-size imperfect counterpart computed by FEM (in black). On the middle and right are depicted the deformed configurations at points a and b, showing also contours of the Lagrangian shear strain component E_{12}. Undeformed configuration is shown by its bounding square. (For interpretation of the references to color in this figure caption, the reader is referred to the web version of this paper.)

convexity). Moreover we can ensure that the critical (i.e. corresponding to the lowest applied load) buckling mode of the infinite, perfect solid is global in nature (infinite wavelength eigenmode), a property that allows us to find a homogenized solution for the bifurcated equilibrium path of the infinite, perfect structure. Within this homogenized framework, we prove that perfect, neo-Hookean composites (incompressible or compressible) of arbitrary fiber/matrix volume fraction, always have a stable initial post-bifurcation response with increasing force and displacement ($\Lambda_2 > 0,\ \lambda_2 > 0$). We also construct a more general composite, consisting of a neo-Hookean fiber and a softer matrix of equal thicknesses which, depending on the constitutive details of the matrix, can exhibit all possible initial post-bifurcation responses: a snap-back ($\Lambda_2 < 0,\ \lambda_2 < 0$), a maximum force ($\Lambda_2 < 0,\ \lambda_2 > 0$) or a stable bifurcation occurring under increasing force and displacement ($\Lambda_2 > 0,\ \lambda_2 > 0$).

The important question addressed next is how a finite-size volume of such a composite will behave in the bulk, i.e. away from its boundaries where strain concentration can easily appear. To this end, we consider a square sample (containing 40 unit cells and using a refined FEM mesh for the corresponding calculations) of the composite with periodic boundary conditions that can capture the homogeneous principal and bifurcated equilibrium paths of the perfect structure. We show, by means of introducing a small geometric imperfection at the middle of the sample, that under these boundary conditions composites with a monotonically increasing force (and displacement) homogenized initial post-bifurcation response ($\Lambda_2 > 0,\ \lambda_2 > 0$) will evolve towards a uniform shearing solution away from the macroscopic critical load and show no localization of deformation pattern past the critical load, in spite of a macroscopic loss of ellipticity of the principal solution. As expected, composites exhibiting the snap-back (i.e. maximum displacement) in their macroscopic response ($\Lambda_2 < 0,\ \lambda_2 < 0$), will evolve into a solution with a single strong localized deformation zone.

The key concept for finding whether loss of macroscopic ellipticity leads to localization of deformation lies in the post-bifurcation behavior of the solid under investigation. Providing consistent criteria based on homogenization ideas, for the absence or presence of localized deformation zones in the post-critical regime of finitely strained solids, is possible, as the current layered composite model shows, for cases when the critical bifurcation mode is also global in nature and well separated from other eigenmodes. For more complex problems, such as solids with 2D or 3D periodic microstructures, the presence or absence of localized deformation patterns cannot be answered by using homogenization ideas, because of the local nature of the bifurcated solutions (finite number of unit cells involved). Instead efficient numerical calculations of their equilibrium paths that take into account the symmetry groups of these structures (both point and space) are needed in order to find their solutions well past the onset of a first instability (see Combescure et al., 2016).

Acknowledgments

This work is dedicated to Pierre Suquet on the occasion of his 60th birthday and attempts to answer a question he posed to the second author a long time ago! The initial part of the work (Triantafyllidis and Santisi d'Avila, 2012) was conducted while M.P. Santisi d'Avila was at the Solid Mechanics Laboratory supported by a post-doctoral fellowship from the Ecole Polytechnique. The work of G. Wen is supported by a Monge Doctoral Fellowship from the Ecole Polytechnique. We also like to thank Prof. Ryan Elliott from the Aerospace Engineering and Mechanics Department at the University of Minnesota for

reading our manuscript and making important improving remarks. Thanks also to the two reviewers for their suggestions and help in improving the clarity of our presentation. All authors are grateful for the support provided by the Ecole Polytechnique.

Appendix A. Critical load of an axially compressed layered solid

A.1. Finite wavelength (local) bifurcation eigenmodes

To find conditions for a non-trivial solution to the system (2.1), (2.2) and (2.3), one can take advantage of its X_1 translational invariance by considering a Fourier transform with respect to X_1. This linear system of partial differential equations and interface conditions with piecewise constant coefficients that governs the onset of bifurcation of the layered solid is thus reduced to the following linear system of ordinary differential equations and interface conditions in X_2:

$$\omega_1^2 L_{i1k1}\hat{v}_k - i\omega_1(L_{i2k1}+L_{i1k2})\hat{v}_{k,2} - L_{i2k2}\hat{v}_{k,22} = 0, \tag{A.1}$$

$$[\![i\omega_1 L_{i2k1}\hat{v}_k + L_{i2k2}\hat{v}_{k,2}]\!] = 0, \quad [\![\hat{v}_i]\!] = 0, \tag{A.2}$$

where $\hat{\mathbf{v}}(\omega_1, X_2)$ is the Fourier transform of $\Delta\mathbf{u}(X_1, X_2)$ and the real number ω_1 is the Fourier transform variable corresponding to X_1. It is assumed that the field $\Delta\mathbf{u}$ is uniformly bounded and has adequate continuity, in which case its Fourier transform $\hat{\mathbf{v}}$ exists in the sense of distributions.

To determine a non-trivial solution $\hat{\mathbf{v}}$ (up to a multiplicative constant), for the periodic system of ordinary differential equations in (A.1) and (A.2), the system is solved on just one unit cell together with some additional boundary conditions at its ends $X_2 = 0^+$ and $X_2 = H^+$. These conditions are provided by Floquet theory, which applies to linear systems of ordinary differential equations in X_2, with periodic coefficients (period is the unit cell thickness H), according to which:

$$\hat{v}_i(\omega_1, H^+) = \exp\big(i\omega_2 H\big)\hat{v}_i(\omega_1, 0^+), \tag{A.3}$$

where the real number ω_2 ($\omega_2 H \in [0, 2\pi)$) is the Floquet parameter of the solution.

The general solution to the system of ordinary differential equations with piecewise constant coefficients (A.1) is found in each layer to be the sum of four linearly independent partial solutions:

$$\begin{aligned}
\hat{v}_k(\omega_1, X_2) &= \sum_{j=1}^{4} \overset{m}{C}{}_k^{(j)} \exp\left(i\omega_1 \overset{m}{Z}_{(j)} X_2 \right); \quad X_2 \in (0, H_m), \\
\hat{v}_k(\omega_1, X_2) &= \sum_{j=1}^{4} \overset{f}{C}{}_k^{(j)} \exp\left(i\omega_1 \overset{f}{Z}_{(j)} X_2 \right); \quad X_2 \in (H_m, H), \\
\hat{v}_k(\omega_1, X_2) &= \sum_{j=1}^{4} \overset{m*}{C}{}_k^{(j)} \exp\left(i\omega_1 \overset{m}{Z}_{(j)} X_2 \right); \quad X_2 \in (H, H + H_m),
\end{aligned} \tag{A.4}$$

where $Z_{(j)}$ ($j=1,4$) are the four complex roots of the following fourth order, biquadratic polynomial in Z:

$$\mathrm{Det}\big[L_{i2k2}Z^2 + (L_{i2k1} + L_{i1k2})Z + L_{i1k1} \big] = 0, \tag{A.5}$$

and $\mathbf{C}^{(j)}$ is the eigenvector of the 2×2 matrix shown in brackets in (A.5) associated with the root $Z_{(j)}$. The eigenvector components $C_1^{(j)}$ and $C_2^{(j)}$ are related by[5]:

$$C_2^{(j)} = D_{(j)} C_1^{(j)}; \quad D_{(j)} \equiv -\frac{L_{1212}Z_{(j)}^2 + L_{1111}}{(L_{1221} + L_{1122})Z_{(j)}}, \tag{A.6}$$

Note that Eqs. (A.5) and (A.6) are valid for each of the two layers and that superscripts m and f are omitted from these equations in the interest of notational simplicity. The requirement that the roots $Z_{(j)}$ are complex for the loading parameter λ of interest, stems from the assumed strong rank-one convexity of each layer, which implies the absence of any discontinuous deformation gradients in each layer for all loading paths considered here.

The Fourier transform of the interface conditions (A.2), after substituting Eqs. (A.4) and (A.6), gives the following equations for the coefficients $\overset{m}{\mathbf{C}}_1$, $\overset{f}{\mathbf{C}}_1$ and $\overset{m*}{\mathbf{C}}_1$ in matrix form:

[5] Repeated indexes in parentheses are not summed, unless explicitly indicated by a summation symbol.

$$\overset{m}{\mathbf{V}}\exp\left(i\omega_1\overset{m}{\mathbf{Z}}H_m\right)\overset{m}{\mathbf{C}}_1=\overset{f}{\mathbf{V}}\exp\left(i\omega_1\overset{f}{\mathbf{Z}}H_m\right)\overset{f}{\mathbf{C}}_1,$$
$$\overset{f}{\mathbf{V}}\exp\left(i\omega_1\overset{f}{\mathbf{Z}}H\right)\overset{f}{\mathbf{C}}_1=\overset{m}{\mathbf{V}}\exp\left(i\omega_1\overset{m}{\mathbf{Z}}H\right)\overset{m_*}{\mathbf{C}}_1, \tag{A.7}$$

for the interfaces $X_2 = H_m$ and $X_2 = H_m + H_f = H$, respectively. The components of the 4×4 matrices $\mathbf{V}$ and $\mathbf{Z}$ are defined by:

$$V_{1j}=1,$$
$$V_{2j}=D_{(j)},$$
$$V_{3j}=L_{1212}Z_{(j)}+L_{1221}D_{(j)},$$
$$V_{4j}=L_{2211}+L_{2222}Z_{(j)}D_{(j)},$$
$$Z_{ij}=\delta_{ij}Z_{(j)}. \tag{A.8}$$

The components of the vector $\mathbf{C}_1$ are the four constants $C_1^{(j)}$ introduced in (A.4). Here again, the superscripts m and f are omitted from (A.8) in the interest of notational simplicity since the components of $\mathbf{V}$, $\mathbf{Z}$ and $\mathbf{C}_1$ are evaluated on the corresponding layer. Substituting Eq. (A.4) into the Floquet conditions (A.3) results in the additional relation:

$$\overset{m_*}{\mathbf{C}}_1=\exp(i\omega_2 H)\exp(-i\omega_1\overset{m}{\mathbf{Z}}H)\overset{m}{\mathbf{C}}_1. \tag{A.9}$$

Finally, after employing the above result (A.9) into Eq. (A.7), a non-trivial solution $\hat{\mathbf{v}}(\omega_1, X_2)\neq 0$ (or equivalently $\overset{m}{\mathbf{C}}_1\neq 0$) exists if the matrix with constant coefficients $\mathbf{K}$ has unimodular eigenvalues:

$$\det[\mathbf{K}(\lambda,\omega_1 H)-\exp(i\omega_2 H)\mathbf{I}]=0;$$
$$\mathbf{K}\equiv\overset{f}{\mathbf{K}}\overset{m}{\mathbf{K}},\quad \overset{l}{\mathbf{K}}\equiv\overset{l}{\mathbf{V}}\exp(i\omega_1\overset{l}{\mathbf{Z}}H_l)\overset{l}{\mathbf{V}}^{-1};\quad l=m,f, \tag{A.10}$$

where $\mathbf{I}$ is the 4×4 identity matrix. It should be noted here that the 4×4 matrix $\mathbf{K}(\lambda,\omega_1 H)$ satisfies:

$$\det[\mathbf{K}]=1,\quad \mathbf{K}^{-1}(\lambda,\omega_1 H)=\mathbf{K}(\lambda,-\omega_1 H), \tag{A.11}$$

and that has real invariants $I_i^K\in\mathbb{R}$, $(i=1,\ldots,4)$. Thus, the critical load parameter λ_c, which represents the first occurrence of a bifurcation in the layered solid during a monotonically increasing loading history, corresponds to the first occurrence of a singular matrix in $(A.10)_1$, as the loading parameter λ increases from zero, over all possible pairs of dimensionless wavenumbers $\omega_1 H$ and $\omega_2 H$.

The calculation works as follows: At criticality $y_c\equiv\exp\left(i(\omega_2 H)_c\right)$ is an eigenvalue of matrix $\mathbf{K}$, and in view of the fact that $|y_c|=1$), it corresponds to the first occurrence of a unimodular root of the following fourth order equation:

$$y^4-y^3I_1^K(\lambda,\omega_1 H)+y^2I_2^K(\lambda,\omega_1 H)-yI_1^K(\lambda,\omega_1 H)+1=0, \tag{A.12}$$

where the two real invariants I_j^K of matrix $\mathbf{K}$, satisfy in view of $(A.11)_3$:

$$I_1^K\equiv\operatorname{tr}\mathbf{K},\quad I_2^K\equiv\frac{1}{2}\left[(\operatorname{tr}\mathbf{K})^2-\operatorname{tr}\mathbf{K}^2\right],\quad I_j^K(\lambda,\omega_1 H)=I_j^K(\lambda,-\omega_1 H). \tag{A.13}$$

For a fixed dimensionless wavenumber $\omega_1 H$, $\hat{\lambda}(\omega_1 H)$ is the lowest value of λ for which the characteristic equation (A.12) admits a unimodular solution for y and corresponds to the first bifurcation load with a dimensionless wavelength $\omega_1 H$ along the X_1-direction. It is given by the lowest positive λ root of one of three equations:

$$\hat{\lambda}(\omega_1 H)=\min\left\{\lambda>0,\ \left|\begin{array}{ll} 2I_1^K-I_2^K-2=0, & (\omega_2 H)_c=0,\\ 2I_1^K+I_2^K+2=0, & (\omega_2 H)_c=\pi,\\ \frac{1}{4}(I_1^K)^2-I_2^K+2=0, & (\omega_2 H)_c=\cos^{-1}(I_1^K/4).\end{array}\right.\right\}. \tag{A.14}$$

The critical load parameter λ_c is then found by a numerical search as the lowest value of $\hat{\lambda}(\omega_1 H)$, when the infimum is taken over an adequately large interval $\omega_1 H\in\mathbb{R}$, in the process also giving the corresponding critical dimensionless wavenumber $(\omega_1 H)_c$, as defined in (2.5). Notice that in view of $(A.13)_3$ only positive wavenumbers $(\omega_1 H>0)$ need to be considered, thus explaining the definition of the critical load in (2.5).

Some additional comments are in line at this point. Depending on whether the infimum in (A.14) occurs at the first, second or third equation, one can determine the nature of the critical eigenmode. More specifically, when the infimum occurs for $(\omega_2 H)_c=0$, the corresponding eigenmode is H-periodic, as shown in Fig. A1d, when the infimum occurs for $(\omega_2 H)_c=\pi$, the corresponding eigenmode is H-antiperiodic, as shown in Fig. A1e, while for an infimum reached at $(\omega_2 H)_c=\cos^{-1}(I_1^K/4)$, the corresponding eigenmode is shown in Fig. A1f.

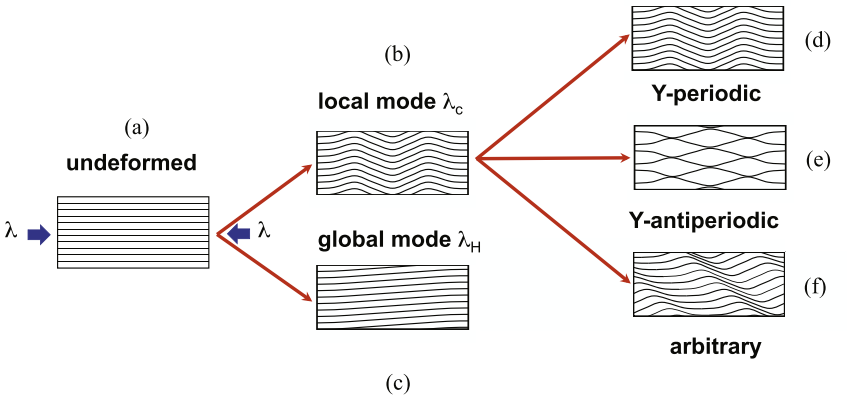

Fig. A1. Different types of bifurcation modes in axially compressed layered media.

A.2. Long wavelength (global) bifurcation eigenmodes

It should be noted here, that in all the previous calculations it was tacitly assumed that the dimensionless wavenumber $\omega_1 H \neq 0$. The function $\hat{\lambda}(\omega_1 H)$ has a singular point at the origin, i.e. $\hat{\lambda}(0) \neq \hat{\lambda}(0^+) \equiv \lim_{\omega_1 H \to 0^+} \hat{\lambda}(\omega_1 H)$, since two physically different types of modes can exist in the neighborhood of $\omega_1 H = 0$: an X_2-periodic, X_1-independent eigenmode $\hat{\mathbf{v}}(0, X_2)$ for $\omega_1 H = 0$ and a long wavelength eigenmode with dimensionless wavelength along the X_1 direction $2\pi/(\omega_1 H) = L_1/H \to \infty$ when $\omega_1 H \to 0^+$. For the latter case it has been shown by Triantafyllidis and Maker (1985), that the limit value of $\hat{\lambda}(\omega_1 H)$, as $\omega_1 H \to 0^+$, is λ_H which corresponds to the loss of rank-one convexity of the homogenized incremental moduli $\mathbf{L}^H$. Although the proof of this assertion for the general case of periodic composites is detailed in Geymonat et al. (1993), for reasons of completeness a brief outline for layered composites in plane strain is presented here.

Starting point for the proof of the above assertion is (A.10), where the asymptotic expansion of $\mathbf{K}(\lambda, \omega_1 H)$ with respect to $\omega_1 H$ gives to first order:

$$
\begin{aligned}
&\det\left[\mathbf{G}(\lambda) - (\omega_2/\omega_1)\mathbf{I}\right] = 0;\\
&G_{11}(\lambda) = G_{22}(\lambda) = G_{33}(\lambda) = G_{44}(\lambda) = 0,\\
&G_{12}(\lambda) = -\langle L_{1221}(L_{1212})^{-1}\rangle, \quad G_{21}(\lambda) = -\langle L_{1122}(L_{2222})^{-1}\rangle,\\
&G_{13}(\lambda) = \langle (L_{1212})^{-1}\rangle, \quad G_{31}(\lambda) = -\langle L_{1111} - (L_{1122})^2(L_{2222})^{-1}\rangle,\\
&G_{24}(\lambda) = -\langle (L_{2222})^{-1}\rangle, \quad G_{42}(\lambda) = \langle L_{2121} - (L_{1221})^2(L_{1212})^{-1}\rangle,\\
&G_{34}(\lambda) = \langle L_{1122}(L_{2222})^{-1}\rangle, \quad G_{43}(\lambda) = \langle L_{1221}(L_{1212})^{-1}\rangle,\\
&G_{14}(\lambda) = G_{41}(\lambda) = G_{23}(\lambda) = G_{32}(\lambda) = 0.
\end{aligned}
\tag{A.15}
$$

Hence (ω_2/ω_1) is an eigenvalue of the matrix $\mathbf{G}$, and must satisfy the following biquadratic equation:

$$
(\omega_2/\omega_1)^4 + (\omega_2/\omega_1)^2 I_2^G(\lambda) + I_4^G(\lambda) = 0,
\tag{A.16}
$$

where the invariants of $\mathbf{G}$ are real and given in terms of its components by:

$$
\begin{aligned}
&I_2^G(\lambda) = -(G_{12}G_{21} + G_{13}G_{31} + G_{24}G_{42} + G_{34}G_{43}),\\
&I_4^G(\lambda) = (G_{12}G_{43} - G_{13}G_{42})(G_{21}G_{34} - G_{31}G_{24}).
\end{aligned}
\tag{A.17}
$$

The critical load parameter corresponding to the long wavelength $\hat{\lambda}(0^+) \equiv \lim_{\omega_1 H \to 0^+} \hat{\lambda}(\omega_1 H)$ is then found as the lowest value of λ for which the biquadratic (A.16) admits real solutions in (ω_2/ω_1), namely the lowest λ root of one of two equations:

$$
\hat{\lambda}(0^+) = \min\left\{ \lambda > 0, \left| \begin{array}{ll} I_4^G = 0, & (\omega_2/\omega_1)_c = 0,\\ \dfrac{1}{4}(I_2^G)^2 - I_4^G = 0, & (\omega_2/\omega_1)_c = \left[-(I_2^G/2)\right]^{1/2}. \end{array} \right. \right\}.
\tag{A.18}
$$

The proof that $\hat{\lambda}(0^+)$ coincides with λ_H, the lowest load parameter corresponding to the loss of the rank-one convexity of the homogenized moduli $\mathbf{L}^H(\lambda)$ follows from (A.15) and (A.16) and the expressions for the homogenized moduli, which are presented next.

For the orthotropic layered medium at hand subjected to axial loading the determination of $\mathbf{L}^H(\lambda)$ starts with the following definition:

$$L^H_{ijkl}(\lambda) = \frac{1}{H}\int_0^H L_{mnpq}\left(\delta_{im}\,\delta_{jn} + \overset{ij}{\varphi}_{m,n}\right)\left(\delta_{kp}\delta_{lq} + \overset{kl}{\varphi}_{p,q}\right)dX_2, \tag{A.19}$$

where δ_{ij} is the Kronecker delta. The characteristic field $\overset{ij}{\boldsymbol{\varphi}}(X_2)$ is the unit cell's response to the ij-th component of the unit macroscopic deformation and is a periodic function in X_2, with period the unit cell thickness H. It is calculated by solving the following boundary value problem given in its variational form:

$$\int_0^H L_{mnpq}\left(\delta_{kp}\delta_{lq} + \overset{kl}{\varphi}_{p,q}\right)\delta\varphi_{m,n}\,dX_2 = 0. \tag{A.20}$$

From (A.19)–(A.20), and recalling the orthotropy of the principal solution, one obtains the following expressions for the nonzero components of the homogenized moduli tensor:

$$\begin{aligned}
&L^H_{1111}(\lambda) = \langle L_{1111} - (L_{1122})^2(L_{2222})^{-1}\rangle + \langle L_{1122}(L_{2222})^{-1}\rangle^2\langle(L_{2222})^{-1}\rangle^{-1},\\
&L^H_{1122}(\lambda) = \langle L_{1122}(L_{2222})^{-1}\rangle\langle(L_{2222})^{-1}\rangle = L^H_{2211}(\lambda),\\
&L^H_{2222}(\lambda) = \langle(L_{2222})^{-1}\rangle^{-1},\\
&L^H_{2121}(\lambda) = \langle L_{2121} - (L_{1221})^2(L_{1212})^{-1}\rangle + \langle L_{1221}(L_{1212})^{-1}\rangle^2\langle(L_{1212})^{-1}\rangle^{-1},\\
&L^H_{1221}(\lambda) = \langle L_{1221}(L_{1212})^{-1}\rangle\langle(L_{1212})^{-1}\rangle = L^H_{2112}(\lambda),\\
&L^H_{1212}(\lambda) = \langle(L_{1212})^{-1}\rangle^{-1}.
\end{aligned} \tag{A.21}$$

The first, as the load parameter increases, loss of ellipticity for the homogenized, layered solid, corresponds to the lowest load parameter λ_H for which the homogenized incremental moduli $\mathbf{L}^H(\lambda)$ lose rank-one convexity, i.e. λ_H is the lowest λ-root of (2.4). From the orthotropy of the homogenized incremental moduli $\mathbf{L}^H(\lambda)$, the determinant of the homogenized acoustic tensor $L^H_{ijkl}(\lambda)n_j n_l$ in (2.6) is the following biquadratic equation:

$$\left(n_2/n_1\right)^4 + \left(n_2/n_1\right)^2 I_2^H(\lambda) + I_4^H(\lambda) = 0, \tag{A.22}$$

where the coefficients I_2^H and I_4^H are expressed in terms of the components of the homogenized moduli tensor by:

$$\begin{aligned}
&I_2^H(\lambda) = (L^H_{1111}L^H_{2222} + L^H_{1212}L^H_{2121}) - (L^H_{1122}) + (L^H_{2222})^2(L^H_{1212}L^H_{2222})^{-1},\\
&I_4^H(\lambda) = (L^H_{1111}L^H_{2121})(L^H_{1212}L^H_{2222})^{-1}.
\end{aligned} \tag{A.23}$$

However, from the expressions for the invariants of $\mathbf{G}$ in (A.15) and the expressions for the components of the homogenized moduli tensor in (A.21) one can show that:

$$I_2^G(\lambda) = I_2^H(\lambda), \quad I_4^G(\lambda) = I_4^H(\lambda), \tag{A.24}$$

thus proving our assertion that $\hat{\lambda}(0^+) = \lambda_H$ and moreover, since the biquadratics in (A.16) and (A.22) coincide, that $(\omega_2/\omega_1)_c = (n_2/n_1)_c$.

A.3. Periodic (X_1-independent) bifurcation eigenmodes

The last case remaining to be checked is $\omega_1 H = 0$, i.e. when the eigenmode is independent on X_1. The corresponding critical load parameter $\hat{\lambda}(0)$ is also found from the transformed governing Eqs. (A.1) and (A.2). In this case it can be seen from (A.1), that $\hat{v}_1(0, X_2)$ and $\hat{v}_2(0, X_2)$ are piecewise linear functions in X_2 within each layer. A nontrivial solution $\hat{v}_i(0, X_2)$ exists when $L_{1212}(\lambda) = 0$ or $L_{2222}(\lambda) = 0$ in either the fiber or the matrix layer, thus giving the critical stretch ratio as the lowest λ root of one of the four equations:

$$\hat{\lambda}(0) = \min\left\{\lambda > 0,\ \middle|\ L^f_{1212}(\lambda) = 0,\ L^f_{2222}(\lambda) = 0,\ L^m_{1212}(\lambda) = 0,\ L^m_{2222}(\lambda) = 0\right\}. \tag{A.25}$$

For the hyperelastic solids investigated here, their rank-one convexity guarantees that $L_{1212}(\lambda) > 0$ and $L_{2222}(\lambda) > 0$ for both fiber and matrix. Even for rate independent solids that might lose ellipticity, one can see that $\hat{\lambda}(0)$ from (A.25) is strictly larger than $\hat{\lambda}(0^+)$ from (A.18), itself being by definition larger than λ_c, the lowest λ-root of (2.5), namely:

$$\hat{\lambda}(0) > \hat{\lambda}(0^+) = \lambda_H \geq \lambda_c \tag{A.26}$$

Note that the existence of a singularity at $\hat{\lambda}$ at $\omega H_1 = 0$ explains the use of the infimum in the definition of (2.5).

Appendix B. Post-bifurcation asymptotics for a compressible neo-Hookean composite

It is now of interest to see if the stability result for the neo-Hookean composite is influenced by compressibility. To this

end we now consider the compressible neo-Hookean composite in (3.3) which also admits a closed form solution. Recalling again from the kinematics in (2.8) that $F_{11}=1-\lambda$ and $F_{21}=\gamma$ one obtains from (2.9) the following expressions for the first Piola–Kirchhoff stresses:

$$\begin{aligned}
&\Pi_{11}=(1-\lambda)\left[\mu-\frac{p^2}{\mu}\right],\\
&\Pi_{22}=0 \quad \Rightarrow \quad p\equiv\mu-k\left[(I_2)^{1/2}-1\right]=\frac{\mu}{1-\lambda}F_{22},\\
&\Pi_{21}=\mu F_{12}+p\,\gamma,\\
&\Pi_{12}=\mu\gamma+p F_{12},\\
&(I_2)^{1/2}=(1-\lambda)F_{22}-\gamma F_{12}=(1-\lambda)^2\frac{p}{\mu}-\gamma F_{12}.
\end{aligned} \tag{B.1}$$

Again recalling shear traction continuity $\Pi_{21}^f=\Pi_{21}^m$ from $(2.9)_3$ and the kinematic constraint $\langle F_{12}\rangle=0$ from $(2.8)_3$ one obtains the following linear system for the two unknowns F_{12}^f and F_{12}^m:

$$\begin{aligned}
&\mu_f F_{12}^f-\mu_m F_{12}^m+(p_f-p_m)\gamma=0,\\
&\zeta_f F_{12}^f+\zeta_m F_{12}^m=0.
\end{aligned} \tag{B.2}$$

The solution of the above linear system for F_{12}^f, F_{12}^m gives:

$$F_{12}^f=\frac{\gamma(p_m-p_f)}{\zeta_f\,\mu_H}, \quad F_{12}^m=\frac{\gamma(p_f-p_m)}{\zeta_m\,\mu_H}, \tag{B.3}$$

where $\mu_H\equiv\left(\mu_f/\zeta_f\right)+\left(\mu_m/\zeta_m\right)$ as defined in (3.11). Using $(B.1)_5$ in combination with (B.3) one obtains the following expressions for p_f and p_m:

$$\begin{aligned}
&p_f=\frac{c_m\left(1+r_f\right)+\gamma^2\left[\left(1+r_f\right)/\zeta_m+\left(1+r_m\right)/\zeta_f\right]/\mu_H}{c_f\,c_m+\gamma^2\left[c_m/\zeta_f+c_f/\zeta_m\right]/\mu_H},\\
&p_m=\frac{c_f\left(1+r_m\right)+\gamma^2\left[\left(1+r_m\right)/\zeta_m+\left(1+r_m\right)/\zeta_f\right]/\mu_H}{c_f\,c_m+\gamma^2\left[c_m/\zeta_f+c_f/\zeta_m\right]/\mu_H},\\
&c_f\equiv\left[(1-\lambda)^2+r_f\right]/\mu_f, \quad r_f\equiv\mu_f/k_f,\\
&c_m\equiv\left[(1-\lambda)^2+r_m\right]/\mu_m, \quad r_m\equiv\mu_m/k_m.
\end{aligned} \tag{B.4}$$

The δ–γ relationship along the bifurcated equilibrium path is obtained from the requirement $\langle\Pi_{12}\rangle=0$ in $(2.9)_2$, and the help of (B.1), (B.3) giving:

$$\langle\Pi_{12}\rangle=\gamma\left[\mu_G-\frac{\left(p_f-p_m\right)^2}{\mu_H}\right]=0. \tag{B.5}$$

Consequently, with the help of (B.4) the sought δ–γ relationship is:

$$c_m(1+r_f)-c_f(1+r_m)=(\mu_G\,\mu_H)^{1/2}\left[c_f\,c_m+\frac{\gamma^2}{\mu_H}\left(\frac{c_m}{\zeta_f}+\frac{c_f}{\zeta_m}\right)\right], \tag{B.6}$$

where without loss of generality it was tacitly assumed that $p_f>p_m$ or equivalently from (B.4) that $c_m\left(1+r_f\right)>c_f\left(1+r_m\right)$. Notice that at the incompressible limit $r_f=r_m=0$, in which case (B.6) reduces to $(3.11)_1$ as expected.

From (B.6) at bifurcation, i.e. for $\gamma=0$, recalling also the definitions of c_f, c_m, r_f, r_m in $(B.4)_3$ which give an additional relation between c_f and c_m:

$$c_m\,\mu_m-c_f\,\mu_f=r_m-r_f\equiv\Delta r, \tag{B.7}$$

one obtains the following result for the critical load λ_c under displacement control $\left(\lambda=-\delta\right)$:

$$\lambda_c = 1 - \left\{ \frac{1}{2}\left[\frac{\Delta M}{(\mu_G\,\mu_H)^{1/2}} + D - (r_f + r_m) \right] \right\}^{1/2},$$
$$\Delta M \equiv \mu_f(1 + r_f) - \mu_m(1 + r_m),$$
$$D \equiv \left\{ \frac{(\Delta M)^2}{\mu_G\,\mu_H} + (\Delta r)^2 + 2\,\frac{\Delta r}{(\mu_G\,\mu_H)^{1/2}} \left[\mu_f\left(1 + r_f\right) + \mu_m\left(1 + r_m\right) \right] \right\}^{1/2}. \tag{B.8}$$

As expected, at the incompressible limit $r_f = r_m = 0$, the above expression reduces to (3.14). The expression for the curvature $\lambda_2\left(\lambda_2 = -\delta_2\right)$ of the bifurcated equilibrium path at the critical point is found by taking the second γ-derivative of (B.6) at $\gamma=0$, giving after some straightforward by lengthy algebra:

$$\lambda_2 = \frac{1}{(1-\lambda_c)D}\left[(1-\lambda_c)^2 + \frac{1}{\mu_H}\left(r_f\,\frac{\mu_m}{\zeta_m} + r_m\,\frac{\mu_f}{\zeta_f} \right) \right], \tag{B.9}$$

which reduces, as expected, to its incompressible limit (3.15) as $r_f = r_m = 0$. Notice that $\lambda_2 > 0$, showing that the compressible neo-Hookean composite has like its incompressible counterpart a stable post-bifurcation response under displacement control.

Appendix C. Influence of constitutive law choice on critical load

In all calculations presented in this work, the response of each layer of the composite is described by a hyperelastic constitutive law, which cannot take into account the presence of a possible unloading in the bifurcated solution. Since unloading will occur in the stiffer layer (matrix), the neo-Hookean model is adequate for this case, due to its linear τ–γ (shear stress–shear strain) response. Hence, to make connections with elastoplasticity, one can compare the predictions of the hyperelastic composites to models where the softer (matrix) layer follows a deformation theory constitutive law, for this layer will continue loading in the homogenized post-bifurcated solution. However, only the onset of bifurcation can be compared for the two different models; post-bifurcation calculations for deformation theory of plasticity would require integrating the corresponding rate-independent (hypoelastic) model, unlike the hyperelastic case where no such integrations are needed.

For comparison purposes we revisit below the composite investigated in Section 3.4, consisting of two equal thickness layers, the stiffer (fiber) being neo-Hookean with energy density $W_f = (1/2)(I_1 - 2)$ and the softer (matrix) being in turn (a) hyperelastic, (b) deformation theory elastoplastic, both sharing the same uniaxial stress–strain law derived from the matrix energy density. For incompressible plane strain conditions, the incremental form of a rate-independent, pressure-insensitive, initially orthotropic material, as first noted by Biot (1965), takes the general form:

$$\overset{\nabla}{\sigma}_{11} = 2\mu^\star D_{11} - \dot{p}, \quad \overset{\nabla}{\sigma}_{22} = 2\mu^\star D_{22} - \dot{p}, \quad \overset{\nabla}{\sigma}_{12} = 2\mu D_{12} = \overset{\nabla}{\sigma}_{21}, \tag{C.1}$$

where $\overset{\nabla}{\boldsymbol{\sigma}}$ denotes the Jaumann rate of the Cauchy stress, $\mathbf{D}$ the strain rate tensor, $\dot{p}$ the hydrostatic pressure rate and the quantities μ and $\mu^\star$ are the incremental moduli associated with an infinitesimal simple shear, superposed on a homogeneous deformation, parallel to the principal axes and at $\pi/4$ respectively. It can be shown (e.g. see Abeyaratne and Triantafyllidis, 1981) that for the deformation theory model proposed by Stören and Rice (1975), which has the same uniaxial stress–strain law as the hyperelastic model (energy density $W = (\alpha/2)g(I_1 - 2)$), only the incremental modulus μ is different between the hyperelastic and deformation theory under loading condition:

$$\mu = \frac{\alpha}{2}\left[(1-\lambda)^2 + \frac{1}{(1-\lambda)^2} \right] g'(z), \quad \text{hyperelastic model},$$
$$\mu = \frac{\alpha}{4\ln(1-\lambda)}\left[(1-\lambda)^2 - \frac{1}{(1-\lambda)^2} \right] g'(z), \quad \text{deformation theory model}, \tag{C.2}$$

where $z \equiv I_1 - 2 = (1-\lambda)^2 + (1-\lambda)^{-2}) - 2$.

Using the matrix energy density from (3.17) in conjunction with (C.2), one obtains the following expressions for the critical load under displacement control λ_c:

$$n\alpha\left[(1-\lambda_c)^2 + \frac{1}{(1-\lambda_c)^2} - 2 \right]^{(n-1)} = \frac{1-(1-\lambda_c)^2}{1+(1-\lambda_c)^2}, \quad \text{hyperelastic model},$$
$$n\alpha\left[(1-\lambda_c)^2 + \frac{1}{(1-\lambda_c)^2} - 2 \right]^{(n-1)} = -\ln(1-\lambda_c)^2 \frac{1+(1-\lambda_c)^4}{[1+(1-\lambda_c)^2]^2}, \quad \text{deformation theory model}. \tag{C.3}$$

Comparing the critical strain λ_c of the composite using the two different matrix models is presented in Fig. C1. As expected from (C.2), since for a given axial strain λ the shear moduli μ are larger for the hyperelastic matrix (while remaining unchanged for the fiber), the stiffness contrast between the two layers is greater for the deformation theory version of the matrix and hence result in a lower critical strain for the corresponding composite.

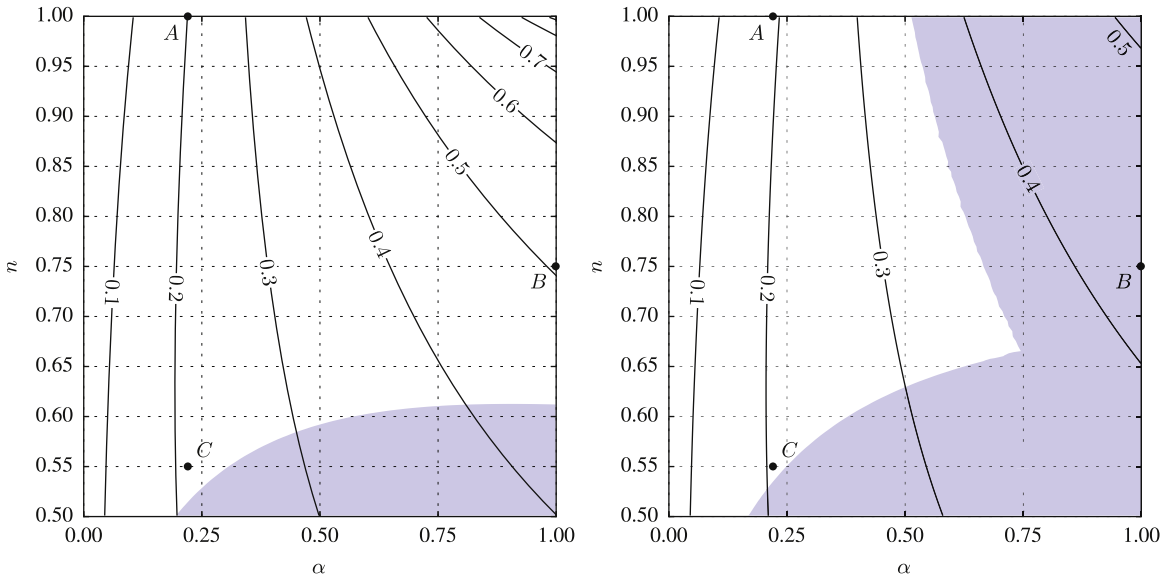

Fig. C1. Critical load (λ_c, in solid black lines) as a function of matrix constitutive parameters for a composite containing two equal thickness layers: a stiff neo-Hookean fiber and a soft nonlinear matrix. On the left figure the matrix is hyperelastic while on the right figure the matrix is based on a deformation theory model of elastoplasticity, with both models sharing the same uniaxial stress–strain response. The blue shaded area in each graph indicates composites where a local bucking mode precedes the global one. (For interpretation of the references to color in this figure caption, the reader is referred to the web version of this paper.)

It is also worth noticing by comparing the shaded areas of the two different composites in Fig. C1 that there is a larger range of material parameters where a local instability precedes the onset of a global one. The bottom shaded area corresponds to antisymmetric local modes (where $(\omega_2 H)_c = \pi$ in (A.14)), while the right shaded area in the deformation theory case corresponds to symmetric local modes (where $(\omega_2 H)_c = 0$ in (A.14)).

An alternative way of comparing the critical strain λ_c of the composite as a function of the initial matrix-to-fiber stiffness ratio α for the two different matrix models for a given hardening exponent (n=0.55, 0.57, 1) is presented in Fig. C2. As explained above, for a given set of material parameters (α, n), the hyperelastic model has a critical load which is consistently higher than its hypoelastic counterpart. However, for small values of α, i.e. large differences between the initial stiffness of the two layers, there is practically no difference between the predictions of the two different matrix models, which means almost identical critical strains in the range $0 \le \lambda_c < 0.2$, as seen in Fig. C2.

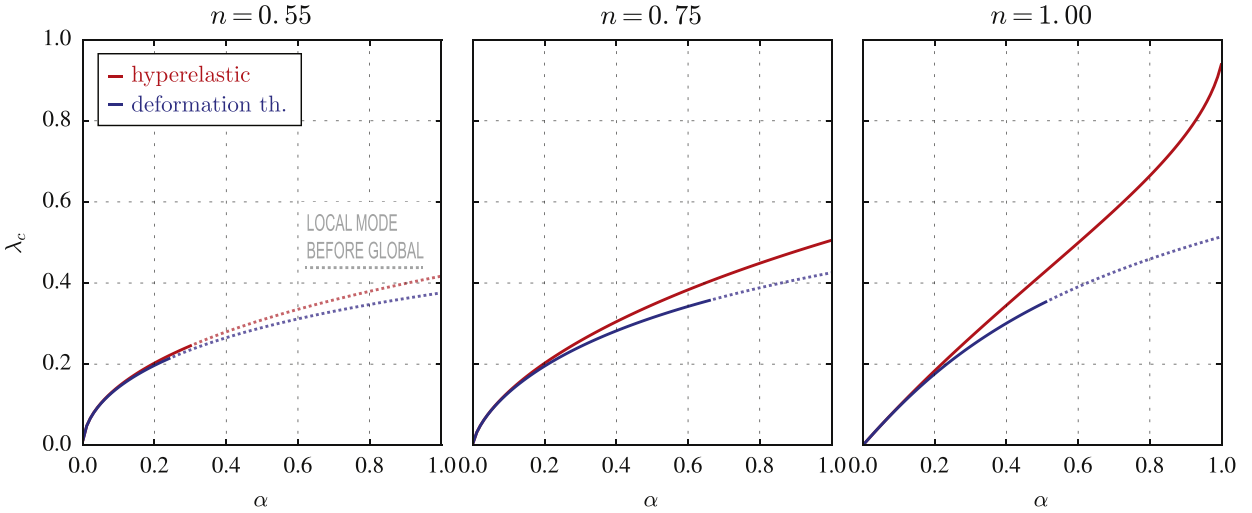

Fig. C2. Influence of constitutive law choice on the critical strain λ_c as a function of the initial matrix-to-fiber stiffness ratio α for the hyperelastic (red line) and the hypoelastic (deformation theory, blue line) matrix models presented in Fig. C1, for three different matrix hardening exponents: n=0.55, 0.57, 1. A solid line indicates a global critical (lowest strain) mode and a dotted line indicates a local one. (For interpretation of the references to color in this figure caption, the reader is referred to the web version of this paper.)

References

Abeyaratne, R., Triantafyllidis, N., 1981. Emergence of shear bands in plane strain. Int. J. Solids Struct. 17, 1113–1134.

Ball, J.M., 1977. Convexity conditions and existence theorems in nonlinear elasticity. Arch. Ration. Mech. Anal. 63, 337–403.

Biot, M.A., 1965. Mechanics of Incremental Deformation. Wiley, New York.

Budiansky, B., 1983. Micromechanics. Comput. Struct., 16.

Budiansky, B., Fleck, N.A., 1993. Compressive failure of fibre composites. J. Mech. Phys. Solids 41, 183–211.

Coenen, E.W.C., Kouznetsova, V.G., Bosco, E., Geers, M.G.D., 2012. A multi-scale approach to bridge microscale damage and macroscale failure: a nested computational homogenization-localization framework. Int. J. Fract. 178, 157–178.

Combescure, C., Henry, P., Elliott, R.S., 2016. Post-bifurcation and stability of a finitely strained hexagonal honeycomb subjected to equi-biaxial in-plane loading. Int. J. Solids Struct. 88-89, 296–318.

Geymonat, G., Müller, S., Triantafyllidis, N., 1993. Homogenization of nonlinearly elastic materials, microscopic bifurcation and macroscopic loss of rank-one convexity. Arch. Ration. Mech. Anal. 122, 231–290.

Gibson, L.J., Ashby, M.F., 1988. Cellular Solids: Structure and Properties. Pergamon Press, Oxford.

Gong, L., Kyriakides, S., Triantafyllidis, N., 2005. On the stability of Kelvin cell foams under compressive loads. J. Mech. Phys. Solids 53, 771–794.

Hadamard, J., 1903. Leçons sur la propagation des ondes et les équations de l'hydrodynamique. A. Hermann, Paris.

Hill, R., 1962. Acceleration waves in solids. J. Mech. Phys. Solids 10, 1–16.

Jang, Y.W., Kyriakides, S., Kraynik, A.M., 2010. On the compressive strength of open-cell metal foams with Kelvin and random cell structures. Int. J. Solids Struct. 47, 2872–2883.

Kailasam, M., Ponte Castañeda, P., 1998. A general constitutive theory for linear and nonlinear particulate media with microstructure evolution. J. Mech. Phys. Solids 46, 427–465.

Kyriakides, S., Arseculeratne, R., Perry, E.J., Liechti, K.M., 1995. On the compressive failure of fiber reinforced composites. Int. J. Solids Struct. 32, 689–738.

Lopez-Jimenez, F., Triantafyllidis, N., 2013. Buckling of rectangular and hexagonal honeycomb under combined axial compression and transverse shear. Int. J. Solids Struct., 50.

Lopez-Pamies, O., Ponte Castañeda, P., 2004. Second-order estimates for the macroscopic response and loss of ellipticity in porous rubbers at large deformations. J. Elasticity 76, 247–287.

Mandel, J., 1966. Conditions de stabilité et postulat de drucker. In: Kravtchenko, P.J., Sirieys, P.P.M. (Eds.), Rheology and Soil Mechanics / Rhéologie et Mécanique des Sols, International Union of Theoretical and Applied Mechanics. Springer, Berlin Heidelberg, pp. 58–68.

Michel, J., Lopez-Pamies, O., Ponte Castañeda, P., Triantafyllidis, N., 2007. Microscopic and macroscopic instabilities in finitely strained porous elastomers. J. Mech. Phys. Solids 55, 900–938.

Michel, J., Lopez-Pamies, O., Ponte Castañeda, P., Triantafyllidis, N., 2010. Microscopic and macroscopic instabilities in finitely strained fiber-reinforced elastomers. J. Mech. Phys. Solids 58, 1776–1803.

Papka, S., Kyriakides, S., 1994. In-plane compressive response of crushing of honeycomb. J. Mech. Phys. Solids 42, 1499–1532.

Papka, S., Kyriakides, S., 1998. Experiments and full-scale numerical simulations of in-plane crushing of a honeycomb. Acta Mater. 46, 2765–2776.

Papka, S., Kyriakides, S., 1999a. Biaxial crushing of honeycombs—Part I: experiments. Int. J. Solids Struct. 36, 4367–4396.

Papka, S., Kyriakides, S., 1999b. Biaxial crushing of honeycombs—Part II: analysis. Int. J. Solids Struct. 36, 4397–4423.

Ponte Castañeda, P., 1991. The effective mechanical properties of nonlinear isotropic composites. J. Mech. Phys. Solids 46, 427–465.

Rice, J.R., 1976. The Localization of Plastic Deformation. Division of Engineering, Brown University.

Rosen, B.W., 1965. Mechanics of composite strengthening.

Stören, S., Rice, J.R., 1975. Localized necking in thin sheets. J. Mech. Phys. Solids 23, 421–441.

Suquet, P., 1983. Analyse limite et homog/'en/'eisation. C. R. Acad. Sci. Paris 296 (II), 1355–1358.

Talbot, D.R.S., Willis, J.R., 1985. Variational principles for inhomogeneous nonlinear media. IMA J. Appl. Math. 35, 39–54.

Triantafyllidis, N., Maker, B.N., 1985. On the comparison between microscopic and macroscopic instability mechanisms in a class of fiber-reinforced composites. J. Appl. Mech. 52, 794–800.

Triantafyllidis, N., Santisi d'Avila, M.P., 2012. Localization and loss of ellipticity in microstructured solids. In: Proceedings of the 23rd International Congress of Theoretical and Applied Mechanics, Beijing, China, vol. 10. ICTAM, Elsevier.

Triantafyllidis, N., Schraad, M.W., 1998. Onset of failure in aluminum honeycombs under general in-plane loading. J. Mech. Phys. Solids 46, 1089–1124.

Vogler, T.J., Hsu, S.Y., Kyriakides, S., 2001. On the initiation and growth of kink bands in fiber composites. Part II: analysis. Int. J. Solids Struct. 38, 2653–2682.

Wilbert, A., Y.-W., J., Kyriakides, S., Foccari, J.F., 2011. Buckling and progressive crushing of laterally loaded honeycomb. Int. J. Solids Struct. 48, 803–816.